ΠΑΝΕΠΙΣΤΗΜΙΟ ΘΕΣΣΑΛΙΑΣ
ΣΧΟΛΗ ΘΕΤΙΚΩΝ ΕΠΙΣΤΗΜΩΝ
ΔΙΑΤΜΗΜΑΤΙΚΟ ΜΕΤΑΠΤΥΧΙΑΚΟ ΠΡΟΓΡΑΜΜΑ
ΠΛΗΡΟΦΟΡΙΚΗ ΚΑΙ ΥΠΟΛΟΓΙΣΤΙΚΗ ΒΙΟΙΑΤΡΙΚΗ
ΚΑΤΕΥΘΥΝΣΗ

«ΥΠΟΛΟΓΙΣΤΙΚΗ ΙΑΤΡΙΚΗ ΚΑΙ ΒΙΟΛΟΓΙΑ»

Λογισμικό για την προσομοίωση διεργασιών θερμικής επιμετάλλωσης

Μαρία Γ. Τζινάβα

ΔΙΠΛΩΜΑΤΙΚΗ ΕΡΓΑΣΙΑ

Επιβλέπων
Κωνσταντίνος Δελήμπασης

Λαμία, 12/11/2019

UNIVERSITY OF THESSALY

SCHOOL OF SCIENCE

INFORMATICS AND COMPUTATIONAL BIOMEDICINE

A software tool for simulating thermal coating processes

Maria G. Tzinava

Master thesis

Supervisor
Konstantinos Delibasis

Lamia

12/11/2019

«Υπεύθυνη Δήλωση μη λογοκλοπής και ανάληψης προσωπικής ευθύνης»

Με πλήρη επίγνωση των συνεπειών του νόμου περί πνευματικών δικαιωμάτων, και γνωρίζοντας τις συνέπειες της λογοκλοπής, δηλώνω υπεύθυνα και ενυπογράφως ότι η παρούσα εργασία με τίτλο «Λογισμικό για την προσομοίωση διεργασιών θερμικής επιμετάλλωσης» αποτελεί προϊόν αυστηρά προσωπικής εργασίας και όλες οι πηγές από τις οποίες χρησιμοποίησα δεδομένα, ιδέες, φράσεις, προτάσεις ή λέξεις, είτε επακριβώς (όπως υπάρχουν στο πρωτότυπο ή μεταφρασμένες) είτε με παράφραση, έχουν δηλωθεί κατάλληλα και ευδιάκριτα στο κείμενο με την κατάλληλη παραπομπή και η σχετική αναφορά περιλαμβάνεται στο τμήμα των βιβλιογραφικών αναφορών με πλήρη περιγραφή. Αναλαμβάνω πλήρως, ατομικά και προσωπικά, όλες τις νομικές και διοικητικές συνέπειες που δύναται να προκύψουν στην περίπτωση κατά την οποία αποδειχθεί, διαχρονικά, ότι η εργασία αυτή ή τμήμα της δεν μου ανήκει διότι είναι προϊόν λογοκλοπής.

Η ΔΗΛΟΥΣΑ

Ημερομηνία

Υπογραφή

Λογισμικό για την προσομοίωση διεργασιών θερμικής επιμετάλλωσης

Μαρία Γ. Τζινάβα

Τριμελής Επιτροπή:

Κωνσταντίνος Δελήμπασης, Αναπληρωτής Καθηγητής (επιβλέπων)

Δημήτριος Ιακωβίδης, Αναπληρωτής Καθηγητής

Βασίλειος Δρακόπουλος, Επίκουρος Καθηγητής

ΠΕΡΙΛΗΨΗ

Οι διεργασίες θερμικής επιμετάλλωσης έχουν συμβάλλει καθοριστικά στον τομέα της βιομηχανίας, καθώς προσφέρουν πολλά πλεονεκτήματα, όπως η θωράκιση από τη φθορά και βελτιστοποίηση των υλικών. Για το λόγο αυτό, έχει γίνει εκτενής ερευνά με στόχο τον υπολογισμό και την πρόβλεψη των κύριων παραμέτρων της θερμικής επιμετάλλωσης, όπως το πάχος της επικάλυψης, βάσει του κινηματικού μοντέλου και άλλων παραμέτρων που εισάγει ο χρήστης. Στο πλαίσιο αυτής της διπλωματικής εργασίας, αξιοποιούνται αλγοριθμικοί υπολογισμοί και μετρήσεις που έχουν εξαχθεί από προηγούμενα πειράματα, ώστε να δημιουργηθεί ένας προσομοιωτής θερμικής επιμετάλλωσης ευρείας εφαρμογής χωρίς γεωμετρικούς ή κινηματικούς περιορισμούς, ο οποίος μπορεί να υπολογίσει το πάχος επιμετάλλωσης ως συνάρτηση της γωνίας πρόσπτωσης, την απόσταση του αντικειμένου από το ακροφύσιο και την ταχύτητα επιφανείας του ίχνους στο σημείο πρόσπτωσης.

Ο προσομοιωτής που παρουσιάζεται στην παρούσα διπλωματική εργασία έχει τη δυνατότητα επεξεργασίας ενός δοκιμίου αυθαίρετης γεωμετρίας με μεγάλη πολυπλοκότητα, το οποίο πρέπει να είναι σε μορφή τριγωνοποιημένης επιφάνειας. Υποστηρίζονται επίσης, η περιστροφή του αντικειμένου, καθώς και η κίνηση και αλλαγή διεύθυνσης του όπλου σε όλους τους δυνατούς βαθμούς ελευθερίας. Ο χρόνος επιμετάλλωσης διακριτοποιείται σε χρονικά βήματα προσαρμοσμένης διάρκειας. Για κάθε χρονικό βήμα, τα τρίγωνα της επιφανείας που βρίσκονται εντός της δέσμης επιμετάλλωσης αναγνωρίζονται και εκείνα που κρύβονται από τη δέσμη αποκλείονται. Για τα εναπομείναντα τρίγωνα, υπολογίζονται οι απαραίτητες παράμετροι επιμετάλλωσης (γωνία πρόσπτωσης, απόσταση του αντικειμένου από το ακροφύσιο και ταχύτητα επιφανείας του ίχνους στο σημείο πρόσπτωσης), ώστε να προκύψει το πάχος της επιμετάλλωσης. Επιπλέον, υποστηρίζεται ο υπολογισμός του πάχους επιμετάλλωσης με χρήση Γκαουσιανού ακτινικού προφίλ έντασης της δέσμης, δίνοντας πιο ρεαλιστικά αποτελέσματα και επιτρέποντας μερική επικάλυψη, η οποία μπορεί να επιλεγεί από το χρήστη.

Τα αποτελέσματα του προσομοιωτή επαληθεύονται, αφού γίνεται σύγκρισή τους με μετρήσεις από θερμική επιμετάλλωση που διεξάχθηκε σε πραγματικό δοκίμιο. Τα αποτελέσματα έδειξαν ότι οι τιμές του πάχους επιμετάλλωσης που προέκυψε από τον προσομοιωτή είναι πολύ κοντά στις αντίστοιχες πειραματικές. Δίνονται, επίσης, ποιοτικά αποτελέσματα για δοκίμια με πιο πολύπλοκη γεωμετρία.

Η χρήση του προσομοιωτή που παρουσιάζεται στην παρούσα εργασία καθιστά δυνατή την πρόβλεψη του πάχους επιμετάλλωσης για πολύπλοκες γεωμετρίες και με τη χρήση πολλών διαφορετικών κινηματικών μοντέλων με μεγάλη ακρίβεια, χωρίς καταστροφικές δοκιμές. Έτσι, μπορεί να χρησιμοποιηθεί ως μια εύκολη και ανέξοδη λύση για τη διασφάλιση ποιότητας και για τη βελτιστοποίηση και τον προγραμματισμό της κίνησης του όπλου, χωρίς πολυέξοδες και χρονοβόρες δοκιμές επιμετάλλωσης, καταστροφικά τεστ και σπατάλη πρώτης ύλης.

SUMMARY

The use of thermal spray coating has become critical in many areas of the industry, as it offers many advantages, with wear protection and material enhancement being the most important ones. For this reason, a lot of research has been made in order to calculate and predict the main parameters of thermal coating spraying process, such as the thickness, based on the kinematic model and the other user controlled operational parameters. In this work, algorithmic calculations and measurements derived from previous experiments are utilized, to propose a general purpose thermal coating software simulator that is able to calculate coating thickness as a function of impact angle, stand-off distance and spot surface speed.

The proposed simulator is capable to handle substrate of any arbitrary geometry of high complexity, provided that is in the form of triangulated surface. Some other supported features are the rotation of the object as well as any movement of the gun and change of direction. Coating time is discretized in elementary time steps of adaptive duration. For every time step, the surface triangles inside the beam are identified and the ones that are hidden from the beam are excluded. For the remaining triangles, the necessary coating parameters (impact angle, stand-off distance and spot surface speed) are computed in order to obtain the resulting coating thickness. There is a mode where a Gaussian profile may be applied to the beam for the calculation of the thickness, giving more realistic results.

The results of the simulator are validated by comparing them with measurements from a thermal spray coating process on a real substrate. The results showed that the simulated thickness approximates very accurately the experimentally measured results. Qualitative results for a substrate of more complicated geometry are also provided.

The use of the proposed simulator makes feasible the prediction of coating thickness for complicated geometries and using different kinematic models with high accuracy, without destructive testing. Thus, it can be used as an easy and inexpensive solution for quality assurance and for the optimization and planning of the gun kinematic, without costly coating trials, destructive testing and raw material waste.

i

ACKNOWLEDGEMENTS

Contents

TERMINOLOGY INDEX

ABBREVIATIONS AND SYMBOLS

$\mathbf{p_g}$	Position vector of the torch
$\mathbf{g}$	Beam unit vector
$\mathbf{B_i}$	Barycenter of triangle i
V_i	i[th] vertex of the object
T_i	i[th] triangle of the object
Π	Plane defined by the point $\mathbf{p_g}$ and vector $\mathbf{g}$ as the normal vector
Y	List of triangles that lie inside the beam
r_0	Beam radius
SoD	The Stand-of-Distance
θ	The impact angle
$\mathbf{n}$	Triangle normal vector
v_{spot}	Spot speed
δt	Time-step
d_i	Distance of the ith barycenter from the axis of the beam
R	The list of hidden triangles
N_p	Size of Y
ω	Angular velocity of object rotation
$\mathbf{v_g}$	Velocity of the gun
$\mathbf{v_{lin}}$	The velocity of the barycenter because of the rotation
th	Coating thickness
g_p	A factor depending on the beam's intensity radial profile
f_t	A multiplier factor for δt calculation
x_{min}, x_{max}	Limits of box scan movement in X axis
z_{min}, z_{max}	Limits of box scan movement in Z axis
x_{par}, z_{par}	The sign of the parity variable for the gun speed
γ_t	Angle of rotation round Z axis

1. Introduction

1.1 Types of wear and need for coating

Wear

Whenever an object contacts another one with or without relative motion to each other, which is very common in nature or in industry processes, wear will occur. Wear is the damaging, gradual physical removal of material at solid surfaces caused by another surface or material. The main reason that wear occurs to an object is the presence of microscopic asperities on its surface. Causes of wear can be mechanical (e.g., erosion) or chemical (e.g., corrosion). In some applications, the wear mechanisms are useful, for instance when changing the surface of an object is needed through grin or polish. In most cases, though wear is unwanted and cost a lot of money to the industries annually. Over the years a lot of effort is made to minimize the impact of wear between the surfaces, but this could be achieved only if the root cause of the failure is known. [16, 19]. The most common categorization is based on the ways of the material removal and these are:

Adhesive wear

Adhesive wear takes place between two surfaces, usually metallic, that are in relative motion with each other, causing friction, and describes in general the unwanted displacement of wear debris from one object and the attachment to the surface of the other one, under load. This type of wear has two subcategories, which are the mild adhesive wear and the severe one. In the first, the debris is created and transferred in a smaller rate, whereas in the second, the rate is bigger and occurs in cases of bigger loads or higher velocities. [16, 20]

Abrasive wear

Abrasive wear occurs when materials is removed from a surface which contacts another surface of greater hardness. The stronger surface may hit or slide across the softer one.

This type of wear is classified based on the type of contact and the environment of the process. The abrasive wear is subcategorized in two-body and three-body abrasive wear. The first occurs when the wear debris or the hard particles are used for the material removal from the weaker surface. Three-body wear occurs when the wear debris is not involved in the process. According to the environment of the contact, the wear is classified as open or closed [20].

Surface fatigue

Surface fatigue occurs when cracking or discontinuities occur at or below a surface, due to cyclic loading at levels below the yield stress of the material. Fatigue wear happens when the wear debris are detached continuous growth of microcracks on the surface. This is achieved by exposing the surface on high or low frequency loading, resulting in low or high fatigue failures respectively.

Fretting wear

Fretting wear occurs by the repetition of cyclically relative surface motion for a long period of time and eventually material will be removed from one or both surfaces in contact. This method, though, can have two serious aftereffects. The first one, which is the most crucial, is when cracks

1

in either surface are created (fretting fatigue) and this can result in catastrophic failure. The second one happens when the fine debris removed by wear are oxidized in air. These are trapped inside the two surfaces and as they are significantly harder, they accelerate the wear damage.

Erosive wear

Erosive wear is associated with the impingement or the impact of particles from a solid, liquid or gaseous stream onto the surface of an object. The angle of impingement is one of the most important factors in this type of wear. In low angle impingement, particles gradually remove material from the surface through continuous deformations and microcutting actions. At high angles, wear occurs due to deformation on ductile materials and due to microcracking at ceramics. [16]

Corrosion wear

Corrosion wear can be seen in both lubricated and unlubricated contacts and is the result of the chemical reaction of a material with a corrosive environment. Corrosion can start from a small area of the object and form crack, or it can extend across a wide area causing the same or different degradation in each part of the surface.

Thermal spray

The term "thermal spray" is used in order to describe a technology which involves several deposition processes for the improvement and enhancement of worn or corroded components. This method is widely used for a very long time, especially by the industry, and over the years, a lot of reasearch is conducted resulting in the optimization and improvement of the field. Because of the constant need for better material characteristics with a low cost of production, the modification of the surface of the materials in order to combine many different features became very appealing. With the deposition of thick coatings on different substrates and with a wide variety of feedstock materials (such as metals, alloys, hardmetals, ceramics and polymers), innovative parts and components with new functionalities were created. Among the benefits of this method, as stated by Fauchais et al. [13] are the following:

− gives the parts increased resistance to extreme conditions by, e.g., increasing the temprature limits in which an object can be exposed through the use of thermal barrier coatings,
− extends the life of component by protecting it from wear due to abrasion, erosion, and corrosion,
− can be used the repairing a worn or partially worn part of a component, offering a cheap solution as replacement of the whole componet is not compulsory,
− offers the opportunity to a low cost material to aquire better properties, only by applying a more expensive and superior coating.

Thermal spray can be divided according to several factors, as stated by Fauchais et al. [13] which are:

2

- the way in which the energy or heat is being exploited in order to cause melting or change in the material's plasticity, so as to form the coating successively. This energy or heat is provided by (i) combustion, (ii) electric discharge, or (iii) by decompressing high-pressure gases (in the case of cold spray),
- the form of the coating material which can be as powder, wires, or rods,
- the atmosphere in which the coating is performed,
- the power consumption and
- the deposition rate.

All these thermal spray techniques are shown below (Fig 1.1), without cold spray process, as it is not actually belong to the category of thermal coating processes.
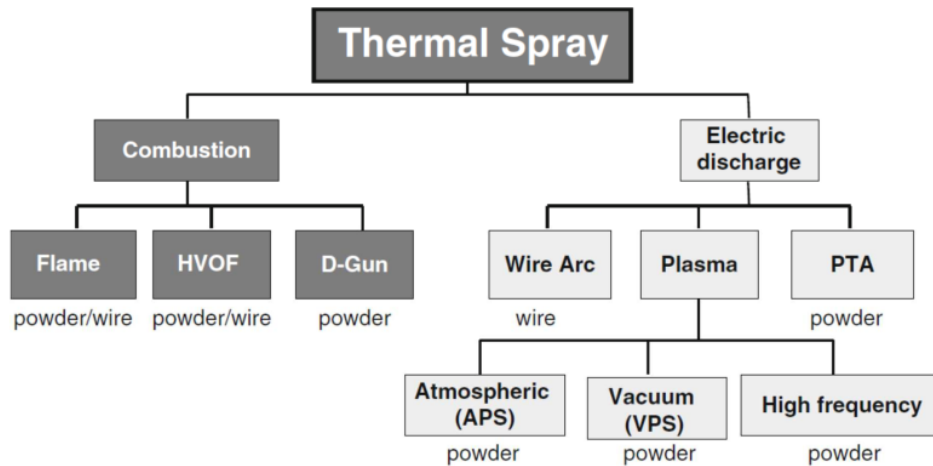

Figure 1.1 Categories of thermal spray techniques [13]

In the 1980s, the thermal spray process called high velocity oxy-fuel (HVOF) spraying was introduced [17], based in internal-confined high-pressure combustion spray process.

This method because of the high gas velocities and low temperatures of deposition, is the most suitable for dense and hard coatings [18].The main deposition method in this work is HVOF so some description of this follows. The HVOF guns have combustion chambers of high pressure, cooled by air or water [16]. A mixture of fuel and oxygen are inserted into the chamber, where they are mixed and ignited continuously. Then the resulting stream of exhaust gases is guided and accelerated through a confined, cooled tube or nozzle forming a jet of high velocity. Powders, are inserted into the nozzle, where particles move through the jet to exit of the nozzle and eventually towards the substrate. In Fig.(1.2) there is a schematic representation of the basic features of HVOF design. An actual HVOF process can be seen in Fig.(1.3).
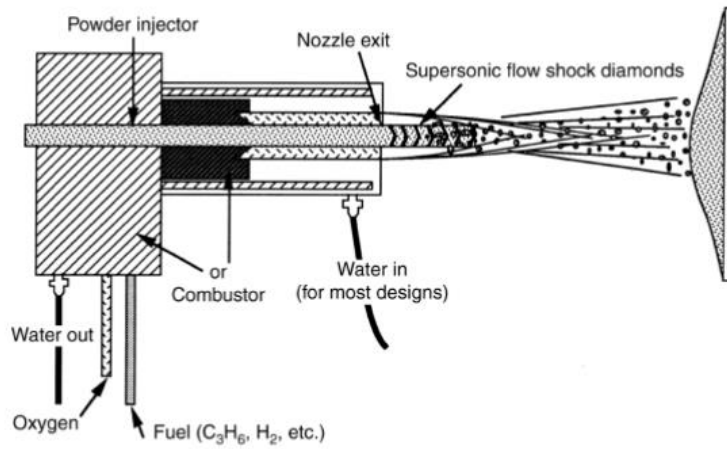
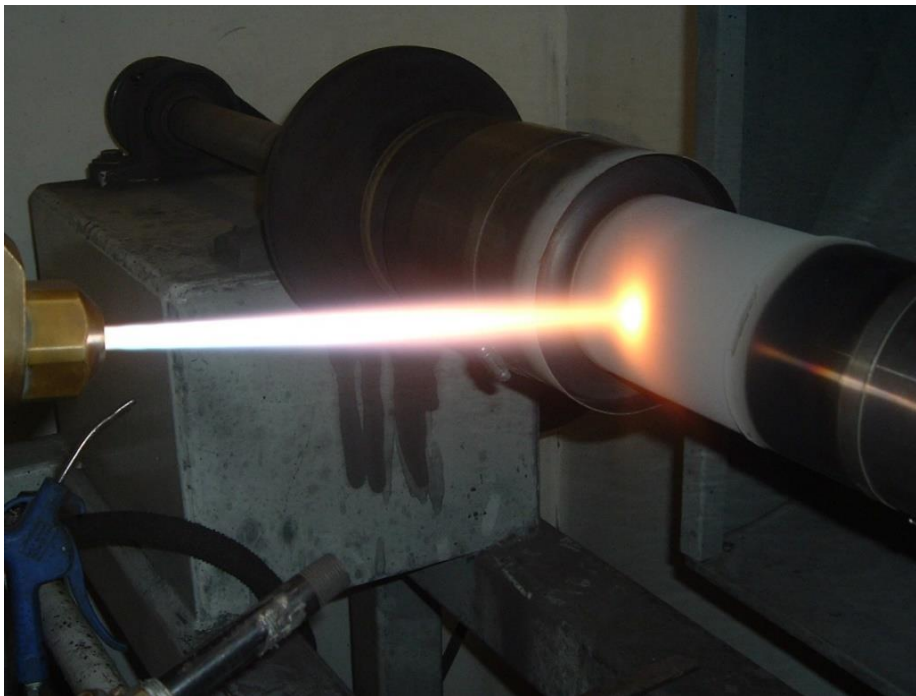*Figure 1.2 HVOF gun schematic representation [16]*

Figure 1.3 The actual process of thermal coating [14]

The main stages of the thermal coating process is shown in Fig.(1.4), in which the powder changes phase and impacts the substrate as high velocity beam resulting in coating.

Figure 1.4 The stages of the thermal coating process [15]

1.2 Literature review of computer based simulations for thermal spray coating

A literature review reveals a limited number of computer based simulations of thermal coating processes. In [1] and [2] experimental results from a coating process with oxy-fuel on geometries with high complexity. Five reference points from a rotating planar geometry are selected, with known values of kinematic parameters (SoD, impact angle, spot speed) and for each point, spraying parameters, such as thickness, porosity, residual stresses and microhardness are measured. Later, in [3] those results were used for the development of a coating simulator. This simulator has several limitations such as, one degree of freedom considering the torch (thus, not allowing torch movement or change of direction) as well as handling geometries which can be expressed as a stack of closed horizontal planar contours in polar coordinates. Thus, complicated shapes that contain holes or discontinuities, cannot be handled. The visibility of each sprayed point from the gun position is also not checked.

In [4] the optimization of the mounting of the nozzle is proposed using a simulation environment (RobotStudio TM). More specifically, kinematic parameters like nozzle speed and the position of the robotic arm joints, are considered, in cases of very simple substrates, like planar plates.

This article [5] suggests a post optimization of the gun kinematic using a deposition model to simulate the coating process. Given specific gun trajectories and poses, the nonlinear conjugate gradient method is used to find the best route for the nozzle to follow in order to optimize the coating error (against user-defined desired values) and the smoothness of the path. A very similar work is reported in [6] where the gun trajectory is optimized for free form objects with simultaneous calculation of heat and mass transfer on the object.

In [7] two methods of optimization of the speed and trajectory of the torch for specific coating paths are proposed. The trials take into consideration the difficulties occurred by the weight and complexity of the robotic arm needed to perform the coating. These methods are verified by conducting simulations in RobotStudio TM and experiments.

Offline methods for programming a robotic torch in order to achieve the desirable result with the minimum error in the coating parameters are presented in [8]. By using simulations the trajectory and the speed of the torch are calculated before the actual process.

In [9] a numerical method is suggested to simulate a generation of splat of the liquefied coating material, during plasma coating and to calculate the porosity between overlapping splats. This

5

method ignores the overall object geometry and although it increases simulation accuracy it cannot be used as a general purpose simulator.

A simulation of the flow field from a well-known HVOF gun using a commercial finite volume CFD code to combine numerical combustion and discrete phase models is suggested in [10]. Results show that the turbulent spray flame and the development of supersonic gas flow can be simulated, for different nozzle dimeters, combustion chamber size and droplet diameter.

This article [11] focuses on the development of a coating model for 2-D shapes of alumina-titania targeting to the optimization of Atmospherically Plasma Sprayed (APS) coatings. This is achieved using many different morphologies and creating optimal paths for different cases of coating. An off- line robotic software simulation is used and for more accuracy, a spray deposition model is applied.

In [12] an experimental simulation of interactions on particle-substrate was developed. The target was to observe the behavior of adhesion in cold spray, by examining the morphology of the microstructure after the simulation.

1.3   The objectives of this work

This work approaches the problem of computer simulation of the HVOF thermal spray process in a different and more comprehensive way than most of the relevant literature. The objective of this work is to finalize the calculation of the thickness in a coating process, given the kinematic parameters and to integrate it with a user-friendly interface that will allow its use outside the academic environment.

More specifically the thickness calculation is based on the stand-off distance (SoD), impact angle and surface speed of the beam spot for any given elementary triangle. The proposed simulator should be able to handle geometries with great complexity, as well as generic kinematic model that supports two methods of coating, box scan and free hand and simultaneous object rotation. The object (substrate) should be introduced to the simulator in the form of triangulated surface, which can be altered to a denser grid, for greater accuracy

2. Methodology

Algorithmic input: 3D geometry of the object (substrate)

2.1 Outline of the algorithm

Let any triangulated object consist of a set of vertices $V = \left\{ V_i \in \Re^3, i = 1, 2, ..., N_V \right\}$ and a set of triangular faces T that hold the indices of vertices that form each triangle $T = \left\{ T_i = (i, j, k) \in Z^{+3}, i = 1, 2, ..., N_T \right\}$. Let the position vector of the torch be $\mathbf{p_g}$, whereas it points parallel to vector $\mathbf{g}$. The beam is considered to be cylindrical with a radius r_0. For each triangle T_i in T the coordinates of its barycenter $\mathbf{B_i}$ are calculated.

Let $Y \subseteq T$ be the list of these triangles inside the beam, sorted by the distance of their barycenters from the torch, in descending order. Although the list Y of triangles lies inside the beam, not every triangle in Y can be sprayed by the torch because some may be hidden (the beam may be blocked by other object triangles, closer to the gun). That may happen because of the geometry of the object and the relative position / orientation of the gun. The hidden triangles are identified through a process that checks all the triangles two by two.

For each of the remaining triangles, which are sprayed eventually by the beam, three parameters are calculated: the Stand-of-Distance (*SoD*) defined as the Euclidean distance between the torch and the triangle barycenter, the impact angle (θ), defined as the angle between triangle normal vector $\mathbf{n}$ and the beam vector $\mathbf{g}$ and the speed of the beam's projection on the triangle (spot speed v_{spot}). Then, the coat thickness can be calculated and added to the coating accumulator, a data structure that accumulates the value of the coating thickness for every triangle in T, over all the iterations of the algorithm.

The above process is repeated through many iterations until the whole substrate is coated. During each iteration the substrate may be rotating and/or the gun may be allowed to change its position $\mathbf{p_g}$ and orientation $\mathbf{g}$ following a predetermined route. For this purpose, the proposed algorithm uses an internal time-step variable δt that defines the object rotation and the gun position and orientation change. Variable δt is adaptively modified during the simulation, according to the geometry of the triangulated object and the frequency of object rotation and gun speed, in order to minimize the execution time, as it will be described later.
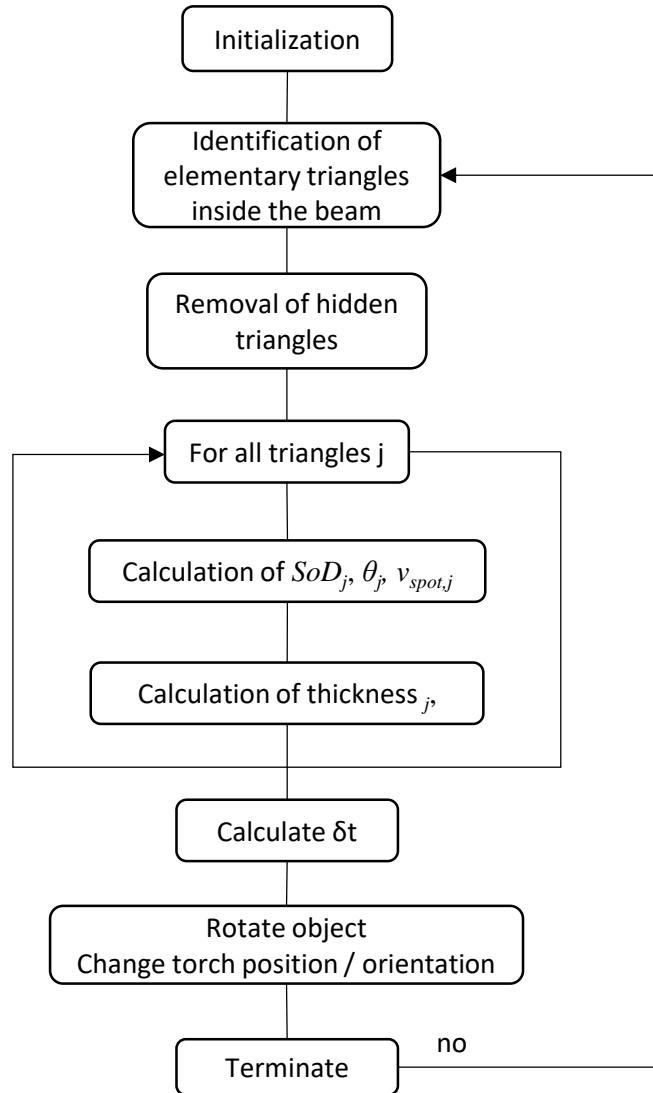
7

Figure 2.1 Schematic representation of the proposed algorithm

2.2 Identification of elementary triangles inside the beam

The first step of the process is the identification of elementary triangles that are inside the beam. This is performed by comparing the beam's radius r_0 to the distance d_i of the ith barycenter from the axis of the beam (defined as the line passing through $\mathbf{p_g}$ parallel to $\mathbf{g}$).

$$d_i = \left\| \left(\mathbf{p_g} + t_i \mathbf{g}\right) - \mathbf{B_i} \right\| \quad (2.1) \qquad \text{where } t_i = \left(\mathbf{B_i} - \mathbf{p_g}\right) \cdot \mathbf{g} \quad (2.2)$$

The barycenters must also lie in the correct side of space separated by the plane Π defined by the point $\mathbf{p_g}$ and vector $\mathbf{g}$ as the normal vector.

8

2.3 Hidden triangle detection

Let us define the set of barycenters that satisfy the above conditions: $Y = \{\mathbf{B_i} : d_i \le r_0 \text{ and } t_i > 0\}$ and N_p be the size of the set. The orthographic projection of triangles Y to the plane Π is performed, creating a list of co-planar triangles Y_p. A triangle in Y is hidden by another one if its projection in Y_p intersects the projection of another triangle. Thus, a triangle intersection algorithm ('tri_intersect') has been developed that returns TRUE if two co-planar triangles intersect. Starting from the more distant triangle from the gun, each one is checked if it is hidden by the less distant triangles in Y.

```
Initialize  R = ∅ // the list of hidden triangles
For i=1,..,Nₚ-1
      For j=Nₚ,…i+1
            If tri_intersect(Yₚᵢ Yₚⱼ)
                  Append Yₚᵢ to list R.
Remove the hidden triangles:  Y = Y − R
```

As a last step, all the hidden triangles are removed from the list.

2.4 Calculation of SoD, impact angle and surface speed of the beam spot

In this subsection we describe the calculation of the three quantities required for predicting the instantaneous coating thickness, namely the *SoD,* impact angle and surface speed of the beam spot.

For any given triangle *i* in *Y* the *SoD* and the impact angle θ_i are easily calculated as following ($\mathbf{p_g}$ and $\mathbf{g}$ are defined as above, whereas the triangle index *i* has been dropped in the equations on this paragraph in the interest of simplicity):

$$SoD = \left\| \mathbf{B} - \mathbf{p_g} \right\| \qquad (2.3)$$

$$\theta = \pi/2 - \cos^{-1}(\mathbf{n} \cdot \mathbf{g}) \qquad (2.4)$$

Let us consider a triangle of the substrate surface with its normal vector **n**. The velocity of the gun with respect to the inertial frame of reference is denoted by $\mathbf{v_g}$ and the velocity of the barycenter because of the rotation of the substrate with angular velocity ω, is denoted by $\mathbf{v_{lin}}$.

$$\mathbf{v_{lin}} = \left[-B_y, B_x, 0 \right] \omega \qquad (2.5)$$

Therefore, the total velocity of the gun with respect to the triangle's barycenter is given by:

$$\mathbf{v_{total}} = \mathbf{v_g} - \mathbf{v_{lin}} \qquad (2.6)$$

9

The 3rd quantity required for coating thickness calculation is the speed of the beam's projection on the object's elementary triangle (spot speed, v_{spot}). This quantity can take values form a very wide range, depending of the object's local geometry, the motion of the gun, the rotation of the object. It can be shown that v_{spot} is calculated as following:

$$v_{spot} = \frac{-\|\mathbf{v_{total}} \times \mathbf{g}\|}{\mathbf{n_p} \cdot \mathbf{g}} \qquad (2.7)$$

where $\mathbf{g}$ is the vector of the gun's beam, $\mathbf{n_p}$ is the component of vector $\mathbf{n}$ that is parallel to the plane defined by $\mathbf{v_{total}}, \mathbf{g}$ and $\mathbf{b} = \mathbf{v_{total}} \times \mathbf{g}$

$$\mathbf{n_p} = \mathbf{n} - \frac{\mathbf{n} \cdot \mathbf{b}}{\mathbf{b} \cdot \mathbf{b}} \mathbf{b} \ . \qquad (2.8)$$

The main vectors of Eq.(2.7) are shown of a randomly selected object's triangle in Fig.(2.2).
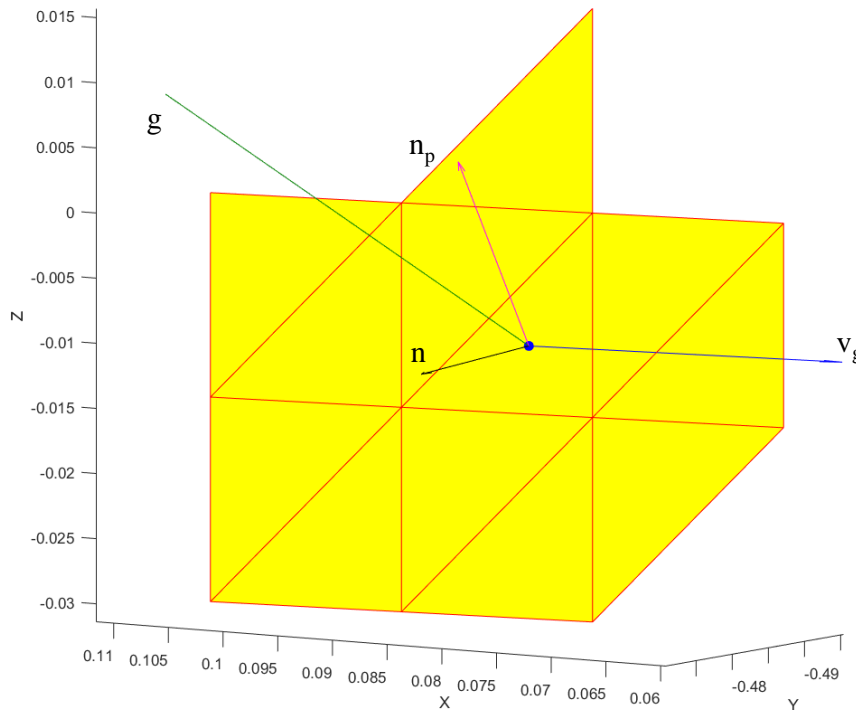
Figure 2.2 Graphic illustration of the vectors used for v_{spot} calculation

2.5 Calculation of thickness value

The value of thickness *th* is a function of the following variables: stand-off distance (*SoD)*, impact angle (*θ*) and spot speed v_{spot}. In [1] thickness measurements are provided for a single kinematic scenario, where the gun is still and coats a plate of appropriate dimensions, rotating at 40rpm:

10

a. Combination of four values of *SoD* in mm (120, 138, 170, 240) and five values of impact angle (90º, 75º, 60º, 45º, 30º).
b. Three different values of spot speed, while keeping *SoD* and impact angle at 120 mm and 90º respectively.

In the most frequent case of non-zero spot speed, $v_{spot} \neq 0$, the following method is applied in order to calculate the thickness of any combination of the three variables. First, hyperbolic interpolation of thickness versus spot speed is performed according to

$$th = f_h\left(v_{spot}\right) = \frac{1}{bv_{spot} + c}, \qquad (2.9)$$

Given the experimental points $\{(v_{spot,i}, th_i)\}$, *i*=1,2,3 the parameters *b*, *c* are estimated *b* =4.8374e-06 and *c* =3.5838e-04, as following:

$$\begin{bmatrix} v_{spot,1}th_1\ th_1 \\ v_{spot,2}th_2\ th_2 \\ v_{spot,3}th_3\ th_3 \end{bmatrix} \begin{bmatrix} b \\ c \end{bmatrix} = \begin{bmatrix} 1 \\ 1 \\ 1 \end{bmatrix} \qquad (2.10)$$

The three experimental measurements of the coat thickness versus the spot speed, as well as the interpolating function of Eq.(2.9) with the resulting parameterization are shown in Fig.(2.3). It can be observed that hyperbolic fit is very accurate.
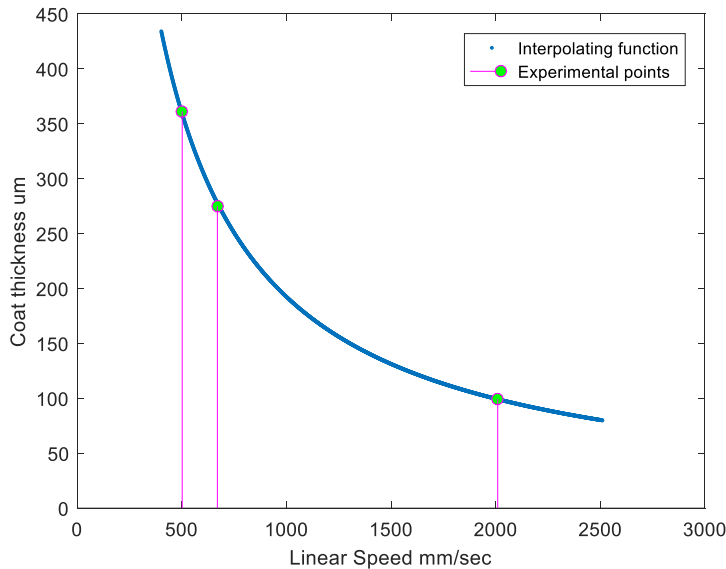
Figure 2.3 The three experimental measurements, the interpolating function and the resulting parameterization combined to calculate the coating thickness

For any combination of the three independent variables (*SoD*, θ, v_{spot}), the resulting thickness is obtained as following. First, we calculate the thickness th_0 for the given *SoD* and impact angle (θ) using bilinear interpolation. The calculated thickness corresponds to spot speed of 502 m/s. In order to convert the thickness to the current spot speed we apply the following:

11

$$th = g_p \cdot th_0 \frac{f_h(v_{spot})}{f_h\left(v_{spot} = 502\right)} \qquad (2.11)$$

Where g_p is a factor depending on the beam's intensity radial profile. More specifically, if the beam's profile is flat, $g_P = 1$. However, in order to obtain more realistic results, a Gaussian profile may be applied to the beam of the gun, thus all the triangles that are inside the beam are not sprayed equally. This factor is calculated for each triangle inside the beam according to the distance d of each barycenter from the beam axis as shown in Eq.(2.12), derived using the Gaussian function with standard deviation $\sigma = r_0/2$.

$$g_p = e^{-\frac{2d^2}{r_0^2}} \qquad (2.12)$$

Under the above profile setting, the intensity of the coating beam at the periphery of the spot is 0.1352 of the intensity in the spot center.

In Fig.(2.4) below, the difference between the coating without the gaussian profile (upper coated area) and with it (lower coated area) can be visually assessed.
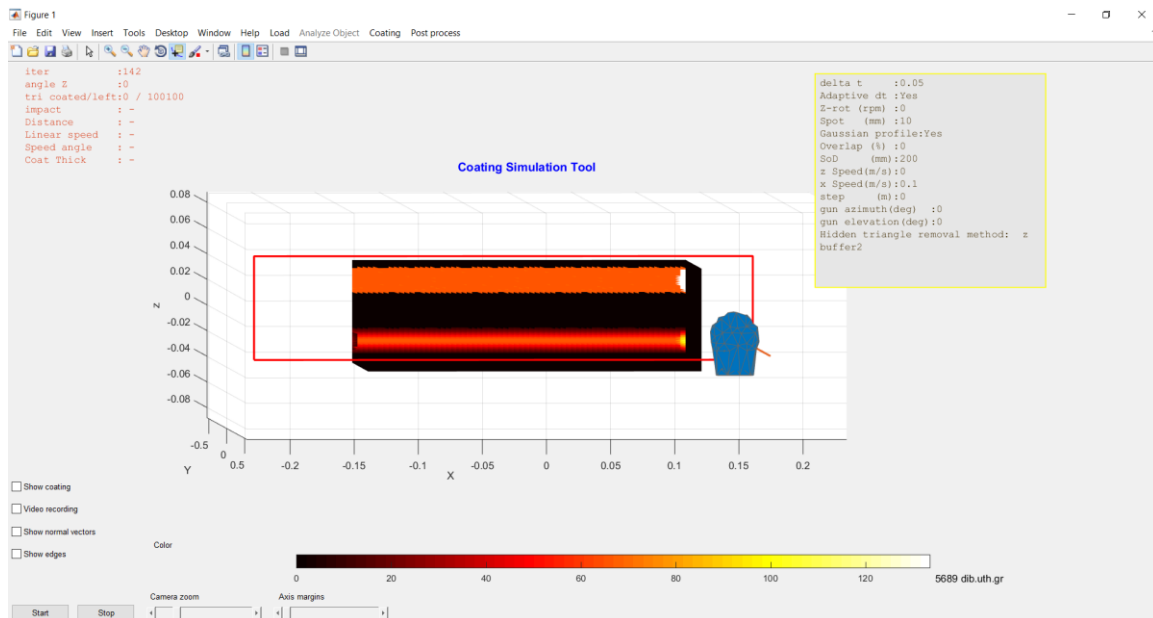
Figure 2.4 Two methods of coating, the upper line is coated without a Gaussian profile and lower with it.

In the case of zero spot speed $v_{spot} = 0$, a situation which can result is both the gun is still and the object does not rotate, or if the gun's speed vector and the linear speed vector (due to rotation) of the triangle being currently coated happen to be equal, coating thickness is considered directly analogous to the coating time step in each iteration (see next subsection).

12

2.6 Determination of the time step δt

In order to accurately simulate the kinematics of the torch and the substrate in an efficient manner, an elementary time step δt has to be defined. If the value of δt is very large, then the coating path on the object will not be continuous, exhibiting gaps (substrate areas that have been skipped). On the other hand, if δt is very small, then the coating will progress very slowly, the same triangles will be "viewed" many times by the same beam spot, thus many duplicate calculations will be performed. In the case of non-zero spot speed, δt is defined adaptively so that the center of the current beam spot on the substrate lies on the periphery of the spot at the previous step. Thus δt is defined adaptively according to the following formula:

$$\delta t = \frac{1}{\|v_{spot}\|}\frac{r_0}{\mathbf{n_p}\cdot\mathbf{g}}\cdot f_t \qquad (2.13)$$

Where r_0 is the radius of the beam, $\mathbf{n_p}$ is defined as in Eq.(2.8) and f_t is a multiplier factor which is usually set to 0.5. If we substitute the expression for v_{spot} from Eq.(2.7) in the above equation, we conclude that δt is independent from the local normal vector.

In order not to allow δt becoming very large, in cases where the v_{spot} is close to zero (due to the reasons mentioned above), the calculation of δt is finally modified, so that it cannot be greater than $\delta t = \frac{r_0}{\|v_g\|}\cdot f_t \qquad (2.14)$

In the case of still gun and non-rotating object, δt is set to a constant value δt_0. Finally, the calculation of that covers all possible cases is given below:

$$\delta t = \begin{cases} \min\left(\dfrac{1}{\|v_{spot}\|}\dfrac{r_0}{\mathbf{n_p}\cdot\mathbf{g}}, \dfrac{r_0}{\|v_g\|}\right)\cdot f_t, & \|v_{spot}\|>0\,OR\,\|v_g\|>0 \\ \delta t_0, & \|v_{spot}\|=0\,and\,\|v_g\|=0 \end{cases} \qquad (2.15)$$

In each iteration the coating thickness is updated only for the triangles that are outside the intersection of the current beam spot with the previous ones and their barycenters are depicted as blue dots in Fig.(2.5). In the special case of keeping the object non-rotating and the gun still the triangle overlap is not checked and all triangles inside the beam are coated with a thickness analogous to the current value of δt.

(a) f_t=0.5

(b) f_t=1

(c) f_t=2
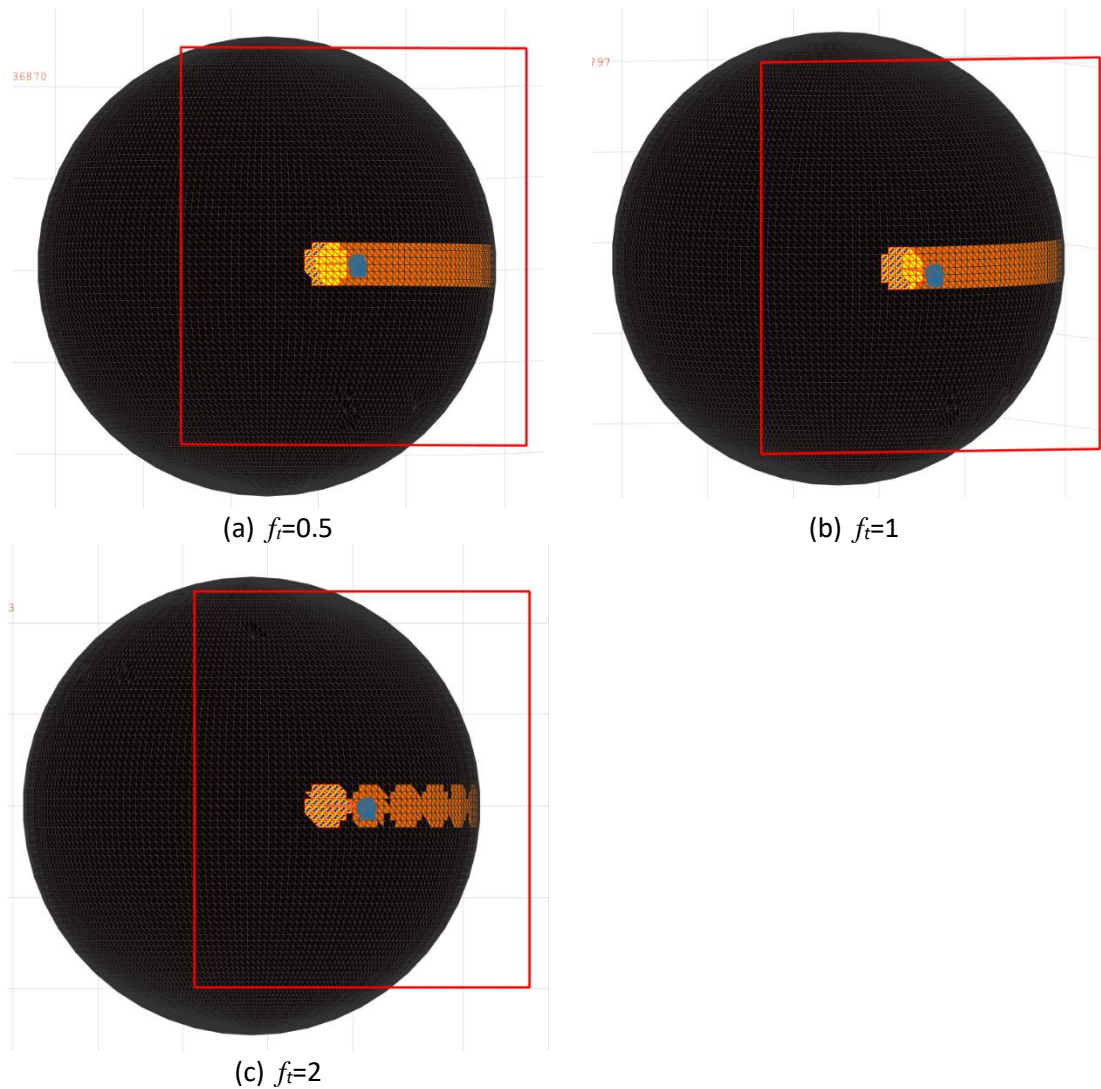
Figure 2.5 The effect of factor f_t in a scenario of coating a sphere, rotating at 100 rpm, using the adaptive δt

A demonstration of the effect of δt on the resulting coating simulation can be seen in Fig.(2.5). More specifically, a sphere of diameter equal to 1 meter is rotated at 100 rpm (round Z axis), while being coated at its equator with a horizontal beam with a diameter of 100 mm.

The beam spot is almost circular because the gun is placed on the plane of the equator. In Fig.(2.5a) the value of δt is automatically calculated according to Eq.(2.13) with f_t=0.5 producing a δt equal to 0.00481sec. It can be seen that, each spot overlaps with the previous one so that the distance between the centers of two consecutive spots is equal to half of the spot radius. In In Fig.(2.5b) and Fig.(2.5c) the value of δt is automatically calculated according to Eq.(2.13) with f_t=1 and f_t=2 respectively.

14
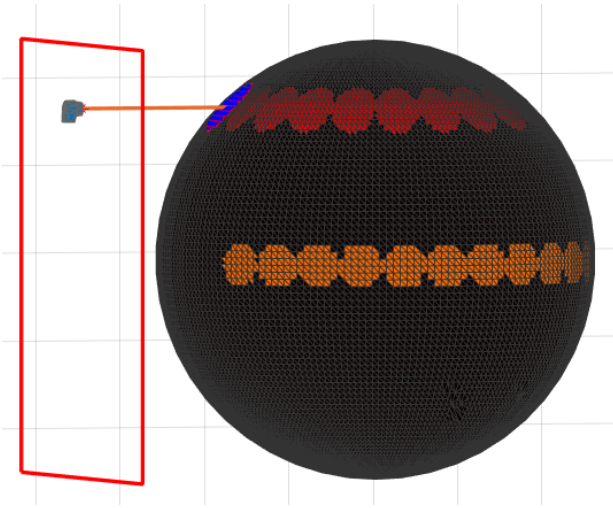
Figure 2.6 Two processes with ft=2.

In Fig.(2.6) the coating process is performed with the same settings and it is simulated using the value of δt obtained by the Eq.(2.13), multiplied by a factor of 2. As expected, the distance between two beam spots is equal to the spot's diameter. Two simulations are performed: in the first one the gun is placed so that the beam is normal to the sphere at its equator (latitude δ=0), therefore the beam spot is circular and δt becomes δt_1=0.019198 s, according to Eq.(2.13). In the second simulation, the beam is also horizontal and intersects with the sphere near its pole, at latitude δ, thus the beam spot is elongated. In this case δt obtains the value of δt_2=0.02685 s, which is larger than the one in the first simulation. According to Eq.(2.7), $\mathbf{g}$ is the same for both cases, $\left\| \mathbf{v_{total,1}} \right\| = \omega R, \left\| \mathbf{v_{total,2}} \right\| = \omega R \cos \delta$ (assuming motionless gun) and the denominator of v_{spot} becomes $\mathbf{n_p} \cdot \mathbf{g} = \cos \delta$. Consequently, v_{spot} is same in both simulations. Thus according to Eq.(2.13), $\delta t_2 = \dfrac{\delta t_1}{\cos \delta}$, equivalently δt increases as the point of impact moves away from the equator (δ =0) towards the poles of the sphere (δ =±90º).

2.7   Calculation of the position and orientation of the gun

By convention, the object is placed so that its major axis is parallel to the Z axis. The object may rotate round Z axis with the center of rotation being the origin of the frame of reference. The software implements two modes for gun movement:

- Box scan and
- Free hand trajectory

In the **box scan mode** there are two allowed axes of gun movement, defined by convention as the X and Z direction, limited by z_{min}, z_{max}, x_{min}, x_{max} respectively, which are defined by the user and may exceed the size of the substrate.

15

The position of the spray gun in *XZ* plane is initialized by default in the middle of the **box scan** selection, with the stand-off distance (*SoD*) of the nozzle initialized at 200 mm (which can be changed by the user). Thus, the spray gun has two positional degrees of freedom. The user can also select the spraying direction, which is expressed in terms of the *azimuth* and *elevation* angle.

The spray gun may move along the X axis with velocity x_{speed} and when it gets close to the limits, (x_{min}, x_{max}), the sign of the parity variable x_{par} is reversed the velocity is reversed, (causing the gun to move in the opposite direction).

$$\mathbf{p_g^{t+\delta t}} = \mathbf{p_g^t} + \delta t \left(x_{speed}, 0, 0\right) x_{par} \qquad (2.16)$$

Then the gun continues moving in the opposite direction alongside the X axis. If there is a step defined by the user, when the gun approaches the X limit, it moves upwards or downwards, depending on its current position, for a distance equal to the step. The aforementioned gun motion can also be applied when the *X* and *Z* axis are interchanged. In the latter case *Z-priority* **box scan**, the gun moves in the same way in *Z* direction with an extra feature. The user can select a minimum and maximum speed. It has to be mentioned here that the instantaneous sign change of the gun's velocity is not very realistic, since in reality the gun first comes to a gradual stop and then it accelerates towards the opposite direction until it achieves the required speed. This actual motion would cause a build-up of coating at the areas of the object that correspond to the gun's movement limits. However, in practice the coating is performed so that the deceleration and acceleration takes place outside the object, therefore, this is currently not considered as a limitation of the proposed simulator.

If needed, the user can change the position of the gun and the spraying angle anytime during the process.

In the **free hand trajectory**, the user may select any number of vertices on the surface of the object and a gun pose is generated by placing the gun at a default distance from the vertex along the surface local normal vector, whereas orienting the gun to point at the selected vertex

A gun trajectory is calculated by moving the gun at preselected default speed through each generated position. The pose (position and orientation) and speed is linearly interpolated between the generated positions.

The user may set the distance and speed from each selected object vertex at any value.

In Fig.(2.7) the two modes of gun movement are shown. In Fig.(2.7a) typical box scan with x priority is performed in a billet with the red line showing the route of the gun. In Fig.(2.7b) the free hand movement is performed in a sphere with the blue lines representing the gun trajectory.
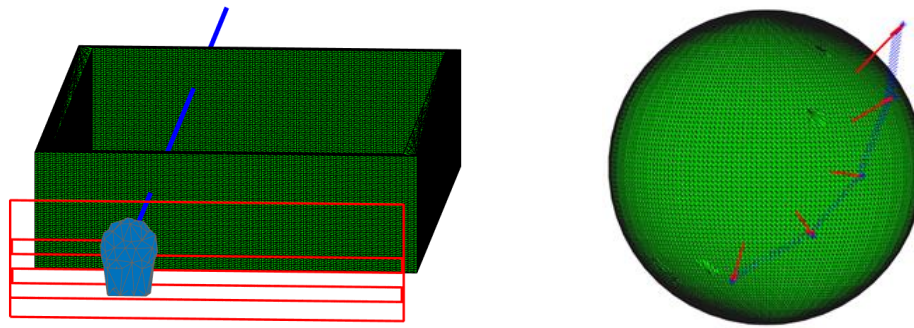
(a) Box scan   (b) Free hand

Figure 2.7 The modes of gun movement

2.8 Update object rotation

As mentioned above the object may rotate during coating with a predefined angular speed ω this rotation is implemented in the simulation as following:

For each iteration the elapsed time t is updated

$$t = t + \delta t \qquad (2.17)$$

The angle of rotation round Z axis is calculated

$$\gamma_t = \omega t \bmod 2\pi \qquad (2.18)$$

The initial vertices of the object are rotated round Z axis as following:

$$\begin{bmatrix} \cos\gamma_t & -\sin\gamma_t & 0 \\ \sin\gamma_t & \cos\gamma_t & 0 \\ 0 & 0 & 1 \end{bmatrix} \mathbf{V}, \qquad (2.19)$$

where $\mathbf{V} = \begin{bmatrix} V_1 & V_2 & \dots & V_N \end{bmatrix}$ and $V_i = \begin{bmatrix} V_{i,x}, V_{i,y}, V_{i,z} \end{bmatrix}^T$.

2.9 Triangle Subdivision

Every object that is used in the simulator has an original triangulation. This triangulation is not always dense enough for the process of coating, though. For this reason, further triangle subdivision is performed as following.

First, a threshold in the length of each triangle is set by the user. By default this is equal to the beam radius. For every triangle in the original triangulation the simulator calculates the number of sides of the triangle that exceed the length of the threshold. The algorithm considers three distinct cases of triangles to be divided, as shown in the schematic representation of Fig.(2.8). In the first case, only one side of the triangle exceeds the threshold. In that case, this side is found and the middle point of the line is calculated and joined with the point of the original triangle that

17

is opposite to it (Fig.2.8a). So, the old triangle is deleted and two new ones are created instead. In the second case (Fig.2.8b), two sides of the triangle exceed the threshold. These two sides are split in half and the middle points are joint together and one of them is joint with its opposite one in the original triangle. Thus, the original triangle is replaced by three new triangles. The third case includes triangles whose all three sides of the original triangle exceed the threshold. In this case, the original triangle is replaced by 4 new triangles, as shown in Fig.(2.8c).

Finally, a check is performed in order to eliminate duplicate points, probably as a result of the procedure described above. Care is taken so that the vertices of the new triangles are ordered in a counterclockwise manner, to preserve the outward direction of the surface normal vectors.
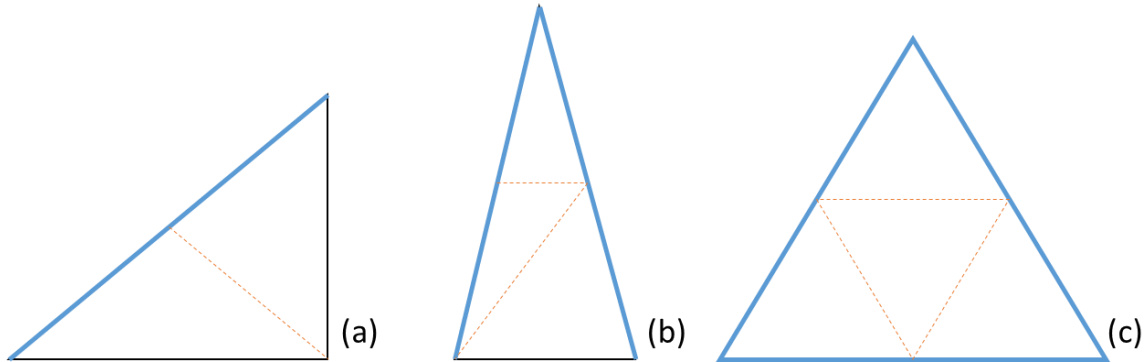
Figure 2.8 Subdivision when a) only one side of the triangle exceeds the threshold, b) two sides of the triangle exceed the threshold, c) three sides of the triangle exceed the threshold.

The subdivision process can be repeated as many times as the user requests.

3. The main features of the software tool

This chapter provides a brief description of the main features of the thermal spray software simulator, which are presented according to the order of the first level menus.

3.1 Load

This menu collects all the input/output operations implemented in the software tool.
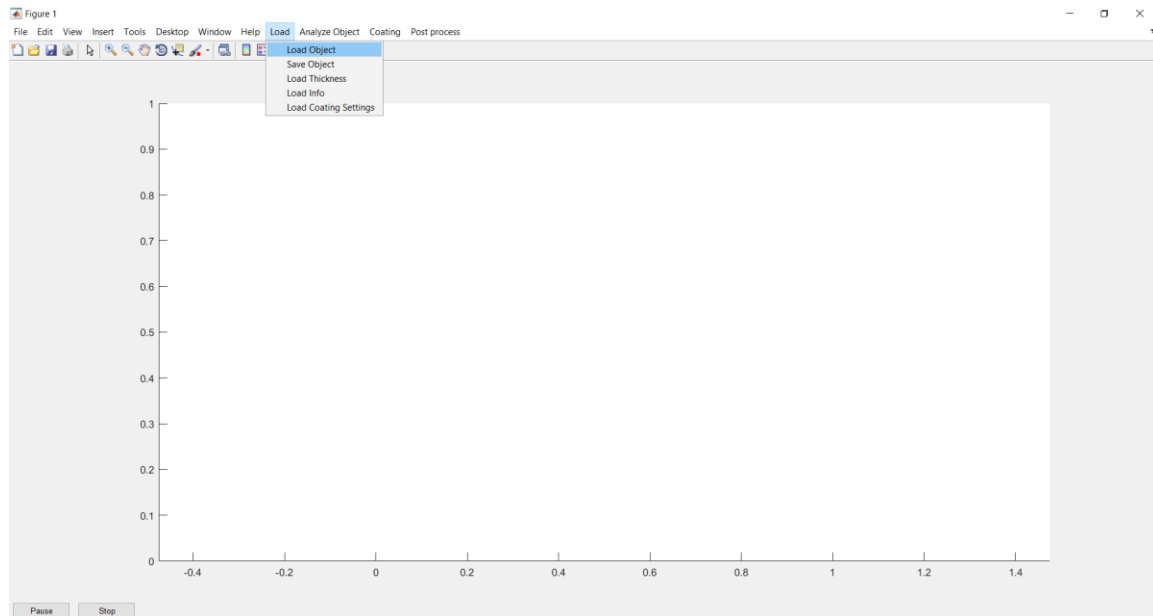
Figure 3.1 Load menu and the layout of the simulator

"Load object"

This selection allows the user to select the object of preference in an .stl format. If the object has been saved by the user in an earlier session, then it will contain a characteristic timestamp, of the form yyyymmddhhmmssfff, (y: year, m: month, d: day, h: hour, m: minute, s: second, f: fraction of the second).

"Save object"

When an object is processed using the simulator certain parameters such as its orientation, scaling, number of vertices and elementary triangles etc. may change. The "Save" option allows the storage of the new object in the .stl format. This simplifies the procedure as the object will be already set the next time the user needs to perform coating.

"Load Thickness"

If a coating process has been already made and saved, the calculated thickness can be loaded, as a .mat file, for further coating or examination. A logical test is performed to check that the number of coat thickness values is the same with the number of triangles in the loaded object.

19

If an object has already been loaded with a timestamp, then the files that are displayed for the user to select must contain the same timestamp and end with the `.mat` extension

"Load info"

This mode offers the capability to store information about a saved coating session in .txt format. This file contains details about every triangle of the object for every passing of the gun. More specifically, the following quantities are saved for each triangle that is visible by the gun's beam in every iteration:

- iteration number
- Number of Rotations
- Angle of rotation round Z axis
- Gun Pos (a 3-element vector)
- Gun beam (a 3-element unit vector)
- the X,Y,Z coordinates of each triangle's barycenter
- Impact angle (deg)
- Stand-off Distance (mm) (of the current triangle barycenter)
- Linear_speed due to rotation (mm/s)
- Surface Spot speed (mm/s)
- Cumulative Coat Thickness (um)
- Current Coat Thickness (um)
- Current time-step dt

"Load Coating settings"

This mode is for loading a .mat file that contains all the parameters needed to perform the coating that has been saved previously. These are

- the way of gun movement,
- the method to find hidden triangles,
- if the time-step is adaptive or predetermined,
- the spot size,
- the rpm of the object,
- the initial stand-off distance of the gun,
- a constant multiplier for calculating the time-step,
- the position and orientation of the nozzle,
- the angle in which was the object just before the stop of the process,
- the total number of rotations the object has made,
- the time-step,
- beam profile (a Gaussian profile),
- the path of the video of the process.

In case of box scan the following are saved additionally

- the speed and direction of the gun,
- the limits of the gun movement,

20

- the overlap in z selection and

In case of free hand movement of the gun the following are saved

- the points from which the gun will pass
- a selected speed for every point
- a stand-off distance for every point

Sometimes in the file of the object, multiple copies of the vertices are created. The option of **merging duplicate vertices** is provided in order to avoid keeping the duplicate vertices, which could result in more processing time.
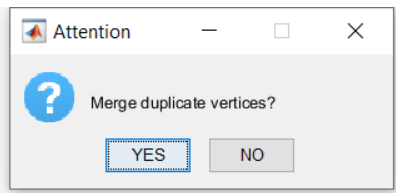
The initial display of the object is shown Fig.(3.2). The axis labels are shown as well as the location of the nozzle, which is depicted as a red star. The preset distance between the object and the nozzle depends on the SoD, it is placed by convention in the middle of the object and in the negative values of y axis.
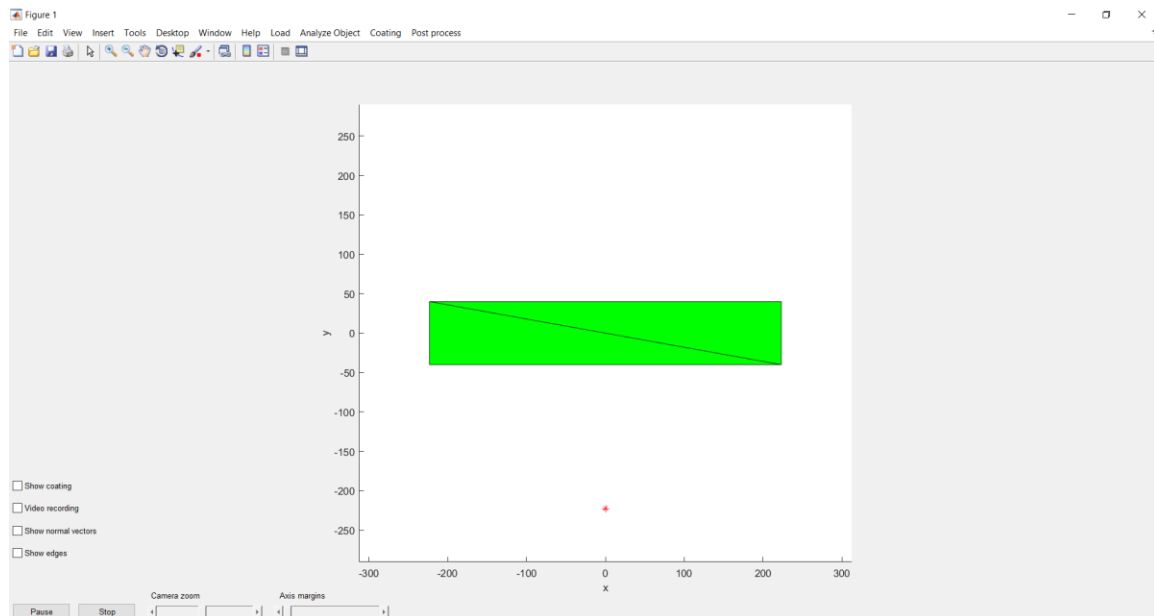
Figure 3.2 Initial display of the object

21

3.2 Analyze object

This menu offers selections for changing the orientation of the object, subdivide the elementary triangles to reduce the triangle sizes, rescale the object to its correct physical dimensions and finally define the motion of the gun in the XZ plane ("Z selection" and "Horiz selection" respectively).

"Orientation"

This selection is used to change the orientation of the object so that the axis of rotation becomes parallel to the Z axis. This necessary in the case of Fig.(3.2), where the current orientation does not allow rotation round the Z axis. Every time that the user selects this option, the object changes its orientation in 3D space by swapping the X, Y and Z coordinates of the vertices in a cyclic-symmetric manner, which can be confirmed by the axis labels. Having them as a guide, the user can select the preferred position of the object.
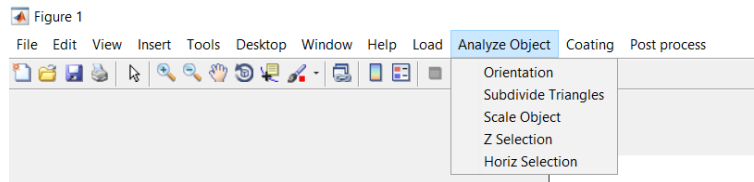
In this position the object is placed and rotated along the z axis. Fig.(3.3) (below) shows the result of this option to the object of Fig.(3.2) (above).
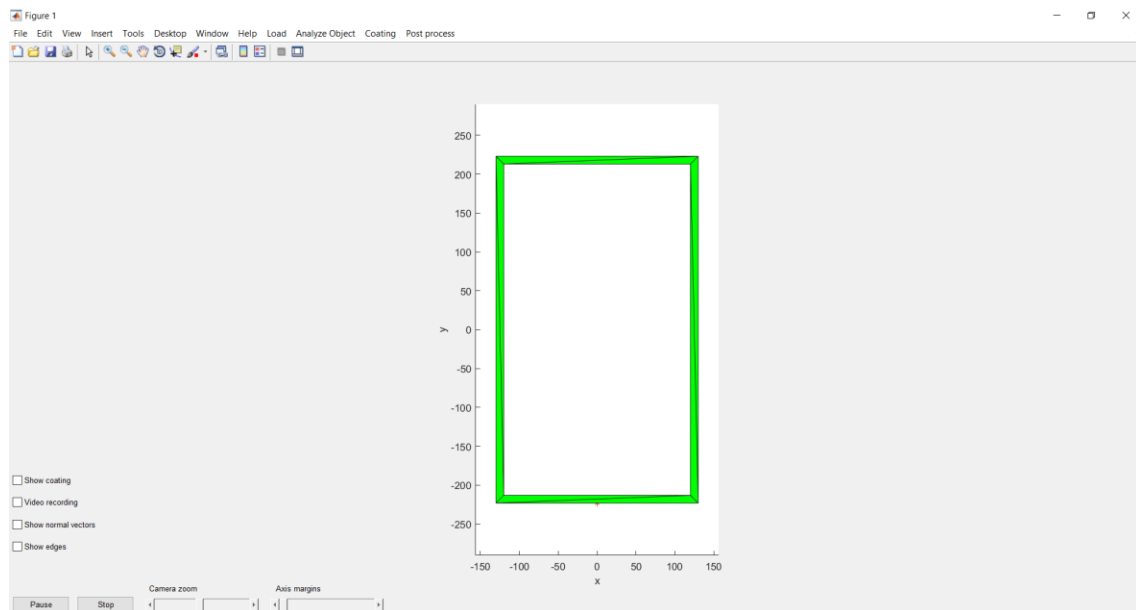
Figure 3.3 The initial object after the change of orientation

22

The user can combine the simulator's options with the standard MATLAB figure tools (such as the 'Rotate 3D' tool) to rotate and examine the object in any direction.
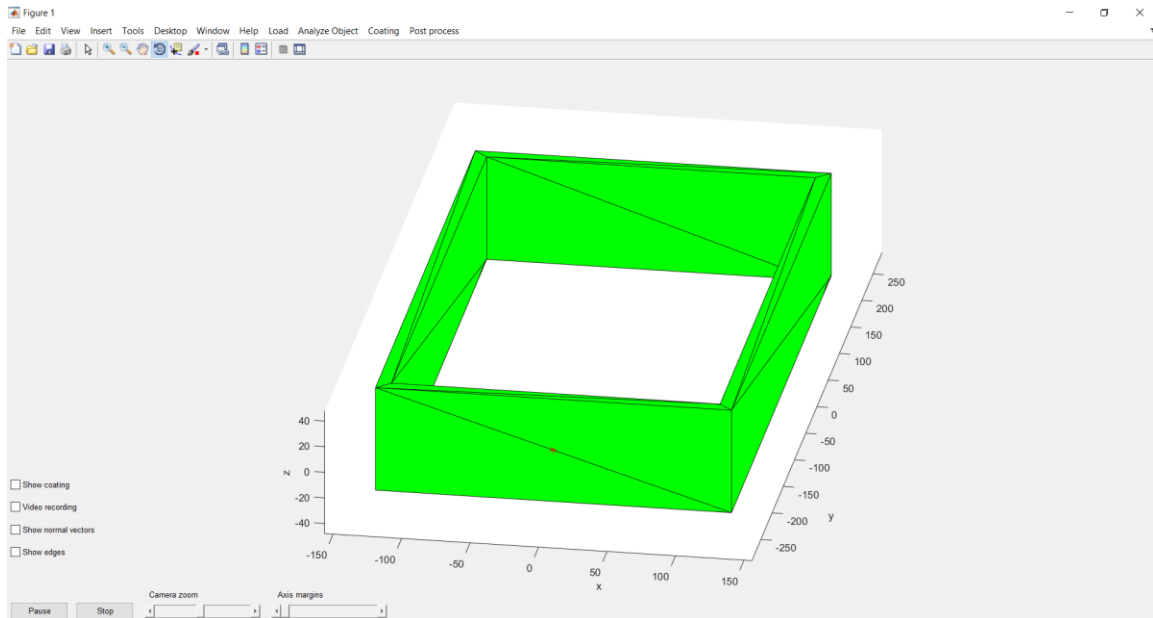
Figure 3.4 A different view of the object using the tool "Rotate 3D"

"Subdivide Triangles"

The triangle subdivision is essential for increased accuracy in coating simulation. The number of subdivisions depends on the object and its initial triangulation, as well as the beam diameter, which is used as a threshold that stops subdivision. The size of triangles should be such that at least few tens of triangles are usually inside the gun's beam. Increasing further the number of triangles will only result in minimum accuracy improvement, whereas drastically increasing computational complexity and execution time. If necessary, the user can decrease the beam diameter (see "Init parameters"), repeat the subdivision as many times as required and then readjust the beam diameter.
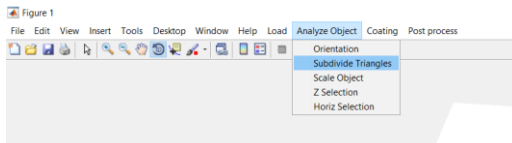
Each time performed, this selection informs the user about the current and the new number of faces and vertices of the triangulation. It also calculates the maximum and minimum size of the triangles' side, as shown below.

23
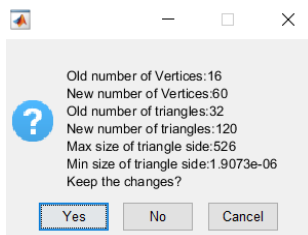
Fig.(3.5) shows the object of Fig.(3.4), after the first invocation of triangle subdivision.
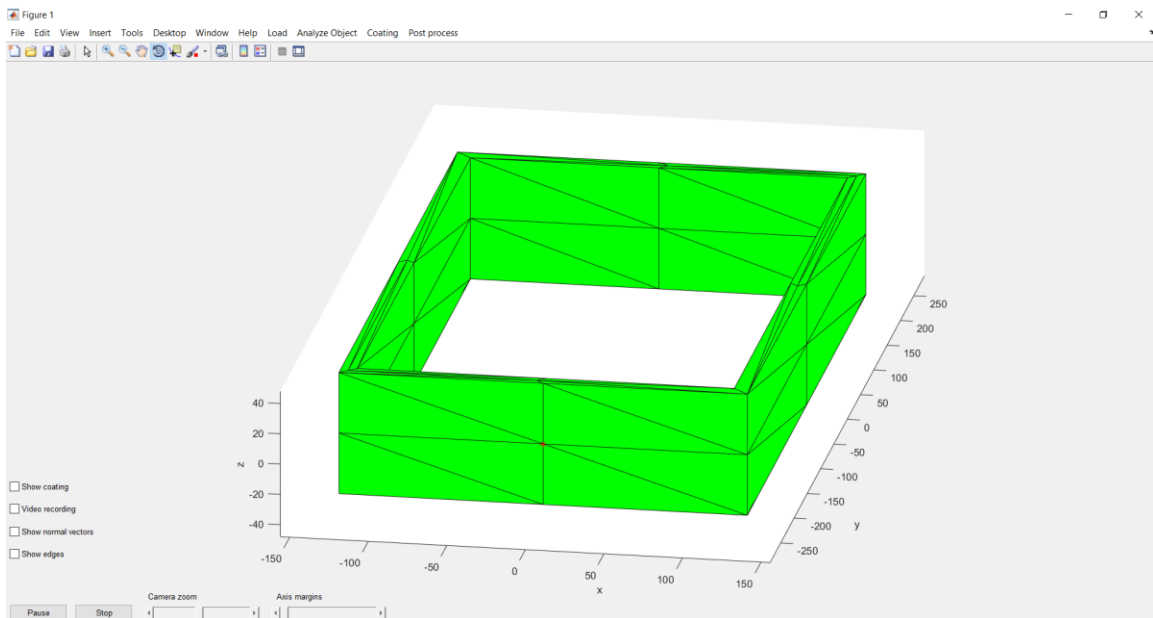
Figure 3.5 The initial object after one application of triangle subdivision

After six application of the triangle subdivision, the object appears as shown in Fig.(3.6).
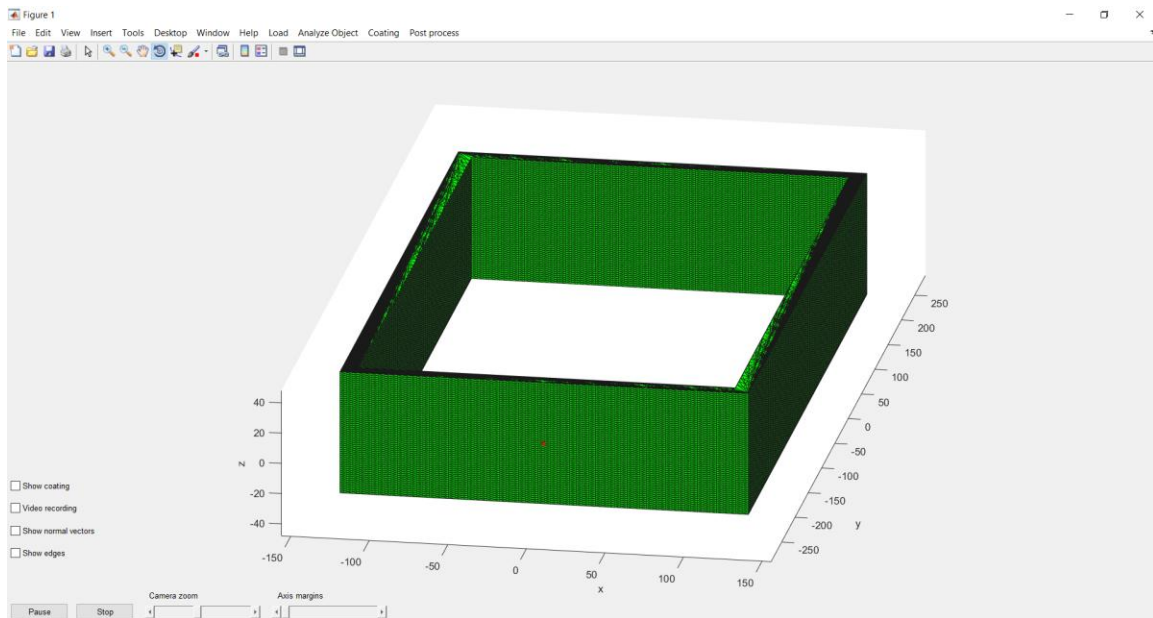
Figure 3.6 The initial object after six applications of triangle subdivision

24

"Scale Object"

When 3D file formats are generated, the units in the vertices' coordinates are arbitrary. The coating simulator however has to operate on physical units of length, time, speed etc. For this reason, the option of "Scale object" has been implemented.

This selection requires the real size of the object in the z axis to be input by the user, in meters. In this way, the coordinates of the vertices are converted from arbitrary units to physical length (meters). The relevant menu is shown below.
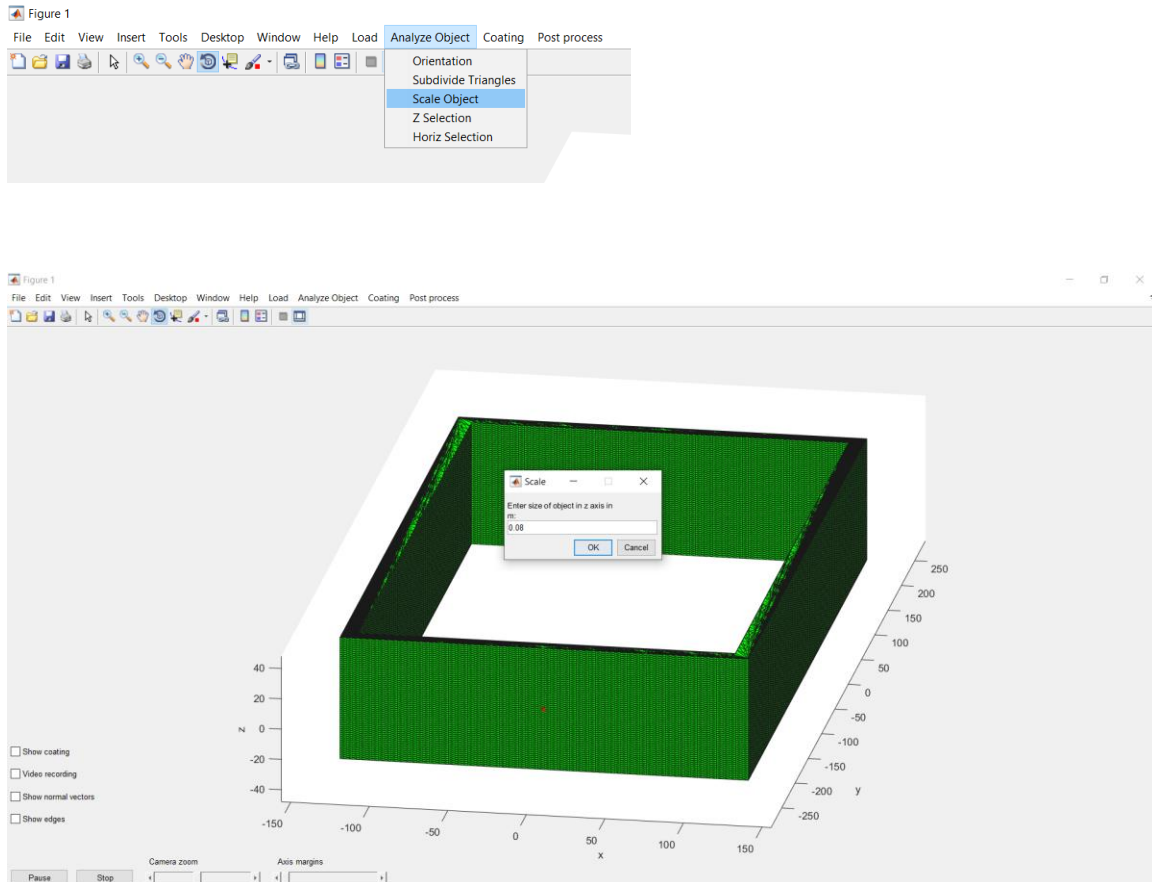
Figure 3.7 The object before scaling with the scale selection window superimposed

In the example of Fig.(3.7), the object before scaling spans the X axis from -140 to +140 units and the Z axis from -20 to 20 units. During the rescale option, the user set the real dimension along the Z-axis to 0.08m, or equiv. 80 mm, which causes all three axes to rescale accordingly, as shown in Fig.(3.8). After the scaling, the nozzle becomes apparent as its dimensions are comparable to the rescaled dimensions of the object. Note that the nozzle is already in real length coordinates and it is not affected by the "Rescale" option.

25
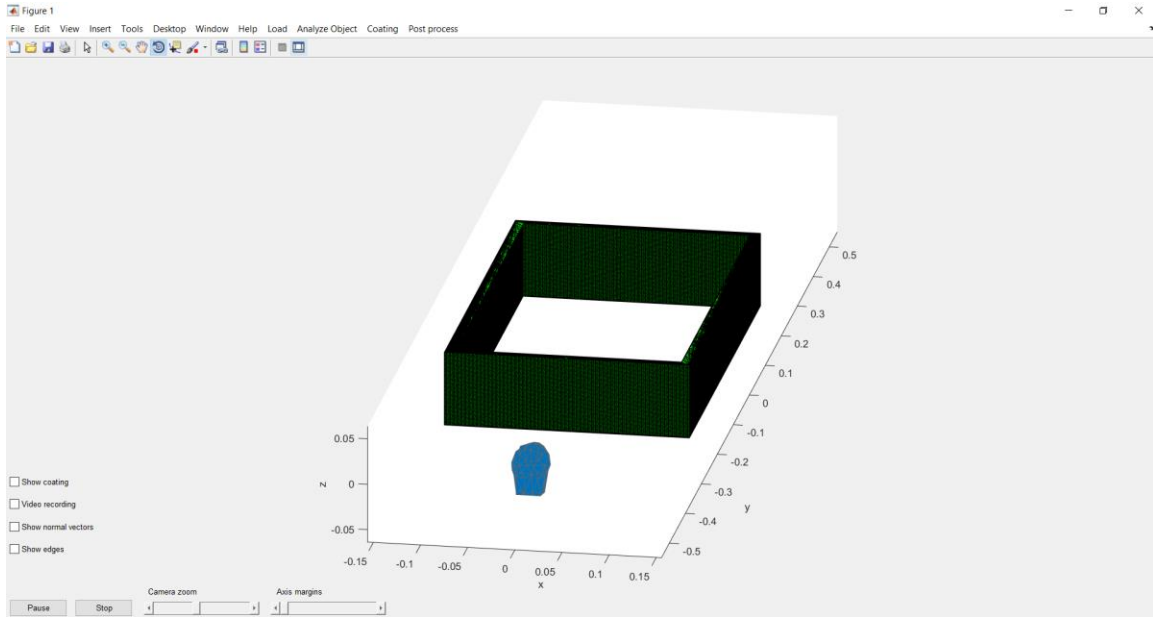
Figure 3.8 The object after scaling and the nozzle after the rescaling

"Z Selection"

This is a selection of the boundaries of the movement of the nozzle in vertical direction.
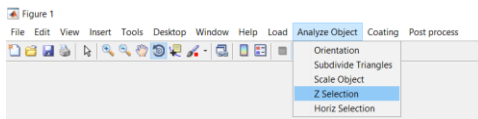
Two scroll bars appear, in order to allow the placement of the limiting vertical planes (left and right). The user may define the X axis limits in numeric format, as well. The selected values are graphically indicated to assist accurate placement.

By moving the two bars the user can find and pick the limits in Z axis. Pressing the "Close" button will store the selected values and remove the scroll bars, as well as the plane graphic depiction in the Fig.(3.9).

26
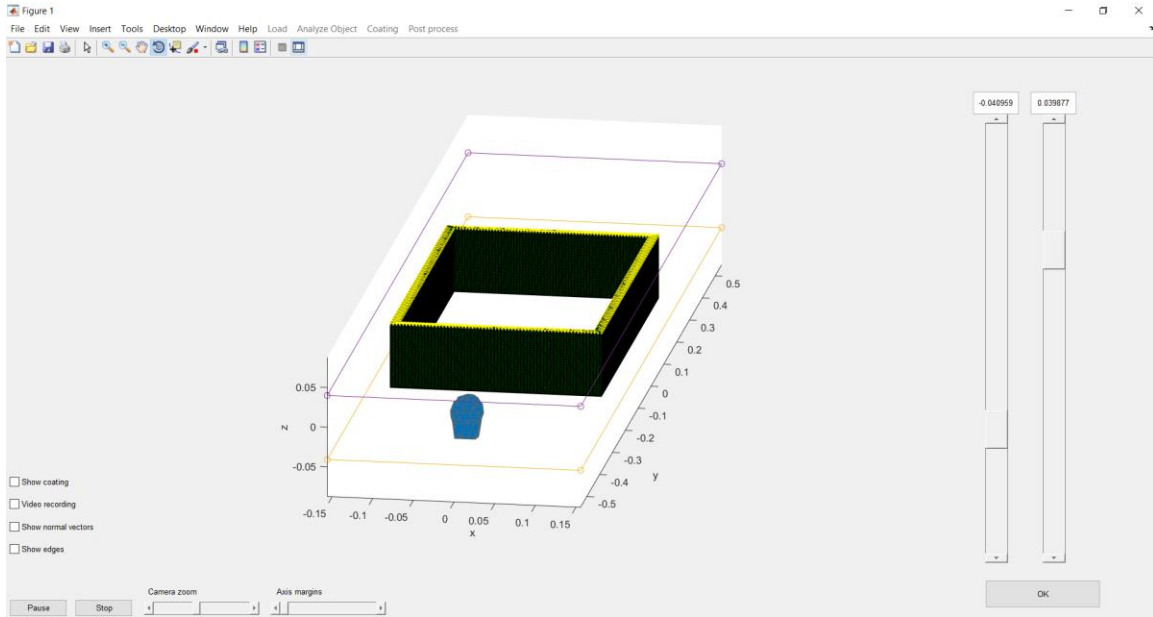
Figure 3.9 The selection of Z axis limits of the gun movement

"Horiz Selection"

This is a selection of the boundaries of the movement of the nozzle in horizontal direction.
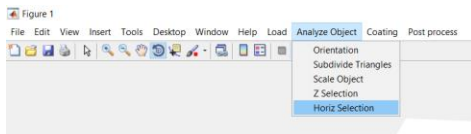
Two scroll bars appear, in order to allow the placement of the limiting vertical planes (left and right). The user may define the X axis limits in numeric format, as well. The selected values are graphically indicated to assist accurate placement.

By moving the two bars the user can set the limits in X axis. Pressing the "Close" button will store the selected values and remove the scroll bars, as well as the plane graphic depiction in the Fig.(3.10).
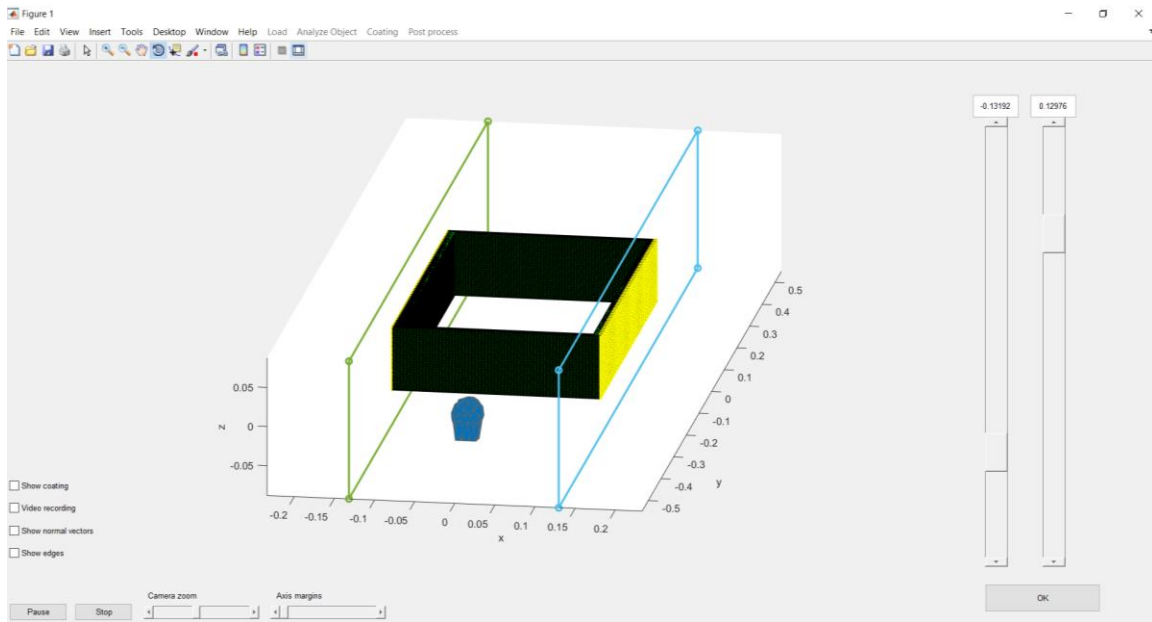
Figure 3.10 The selection of X axis limits of the gun movement

3.3 Coating

The collection of options within this first order menu allows for setting every coating parameter, defining the possible gun motion and object rotation, preview the selected kinematic model before the actual simulation and finally perform the simulation. The following subsections describe the each selection in a more specific manner.

"Init Parameters"

This is a modal window which allows edit of all parameters needed for the coating simulation.
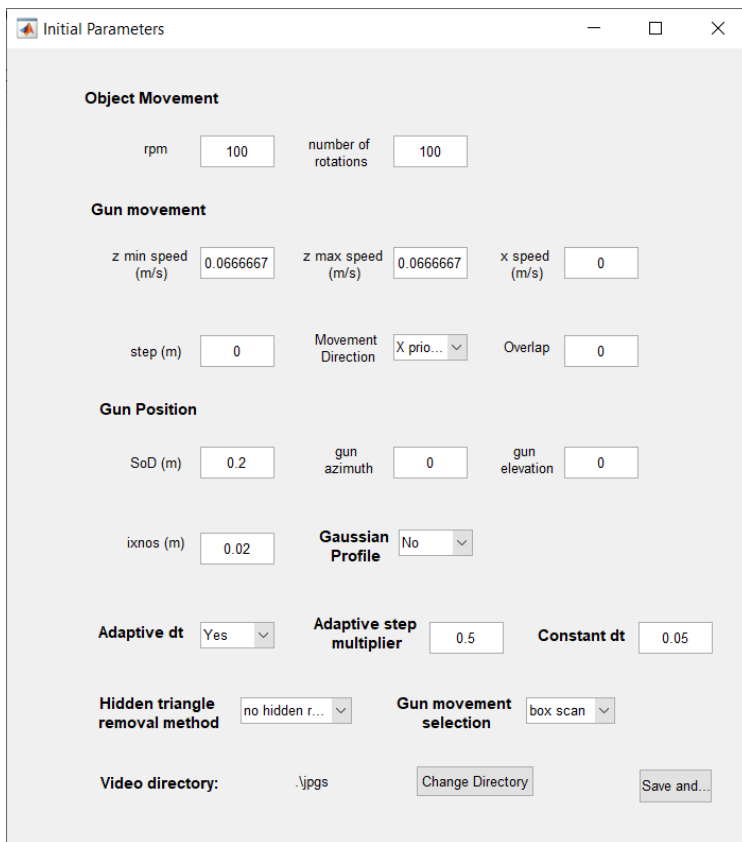
Figure 3.11 The modal window for setting the parameters of the coating simulation

The first group is about the movement of the object: the ***rpm*** as well as the ***total number of rotations*** are selected.

The movement of the gun can be set using a combination of different settings: The type of the motion can be either "**box scan**", or "**free hand**", set by the drop down menu shown below.
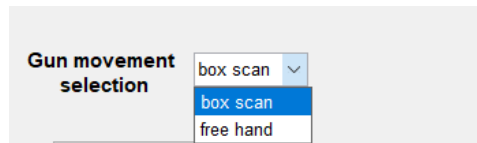
If the "**box scan**" is selected, then the details of the motion are controlled by the setting in Group 2:

In the next group, the movement of the gun can be set. In the Z axis there is an option in which the speed of the gun starts from a certain value "*z speed max*" and increases linearly to another one set in "*z speed min*". If the two values are equal the speed of the gun in Z axis is steady. If the movement of the gun is in X axis the x speed is inserted.

The direction of the movement is selected in the relevant drop down menu: if the gun moves in X direction, X priority is selected, if it moves in Z direction, Z priority is selected. The gun can be allowed to move along both the Z and the X axis, if it is required: the 2nd axis motion is defined by the "step" parameter. *Step* is defined in meters and is the length transversed along the second axis of motion, each time the gun reaches the upper or lower limit along the primary ("priority") axis.

When the object rotation is activated, and the box scan type of motion is selected, the user can choose a certain overlap ratio with respect to spot radius ("*overlap*") along the Z axis. The simulator calculates the appropriate Z speed (m/s) in order for this to be achieved, according to the formula Eq.(2.20):

$$Z_{speed,over} = \frac{\left(2r_o\left(1-\lambda\right)\cdot\omega\right)}{60\pi} \qquad (2.20)$$

Every time the value of overlap or the radius of the beam r_0 changes, the minimum and maximum Z speed value is calculated based on Eq.(2.20) and the text boxes marked in blue in Fig.(3.12) are automatically updated. The user can however overwrite this value if necessary.

Figure 3.12 Interdependent parameters in the modal window

The third group of parameters is the gun position. It includes the stand-off distance, the direction of the gun analyzed in two angles, azimuth and elevation of the gun, and the radius of the beam r_0.

Another parameter defines the profile of the intensity of the coating beam as one of two types: flat (default) and Gaussian with respect to the distance of the beam's central axis.
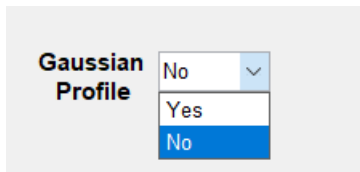
The rest of the available options include:

- Automatic (adaptive) calculation or manual setting of the timestep *dt* and the multiplier used for the calculation, which is described by the Eq.(2.13).
- The algorithm for hidden triangle removal, using a dropdown menu as following: the first option is not to search for hidden triangles and all the triangles inside the beam to be coated. Then three methods for this cause can be used, the quick removal, the extensive search and Z buffer method.
- The path in which the screen shots during the coating process should be saved.

31
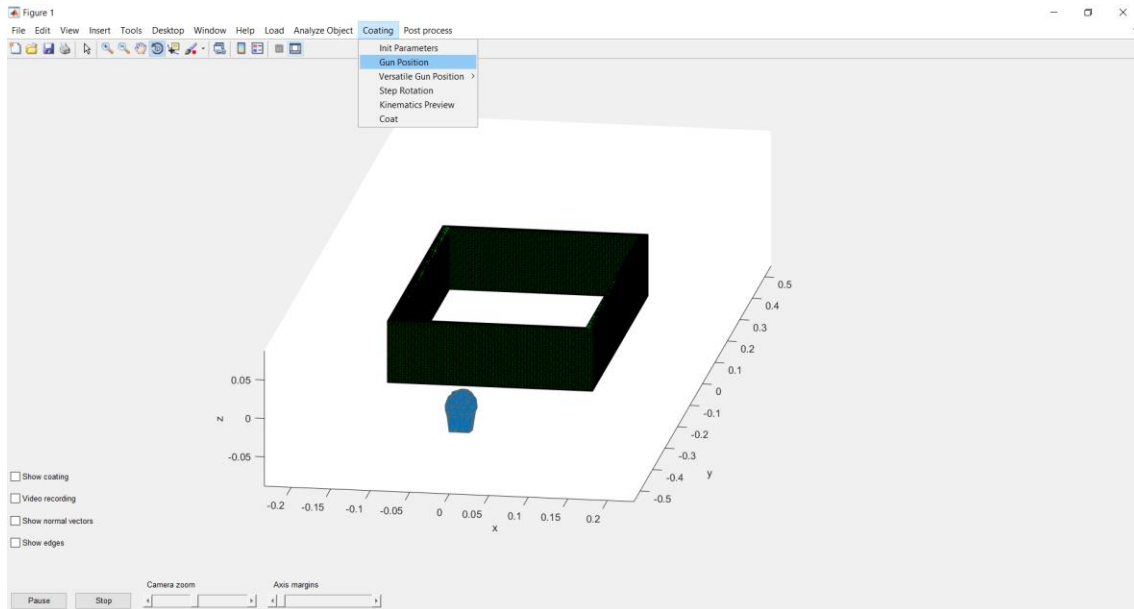
"Gun position"

Figure 3.13 The selection that sets the position of the gun

The user may change the position of the gun, at any point of the coat process (either at the beginning, or during the process after pressing the "Pause" button, using three scroll bars (one for each Cartesian axis). The original nozzle position can be restored by pressing the "*Reset Gun Position*" button, which returns the nozzle in the middle of the red frame and at the negative values of Y axis, at a distance from the object equal to the *SoD*.

Pressing the "*OK*" button will save the selected position and close the scrollbars.
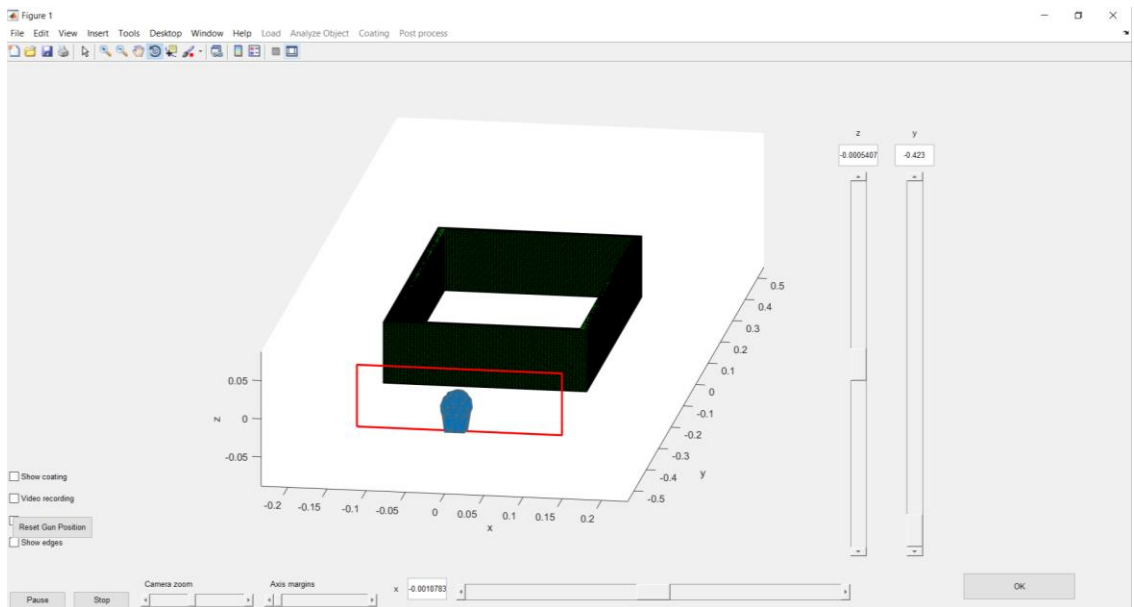
Figure 3.14 The structure of the gun position selection

"Versatile gun position"
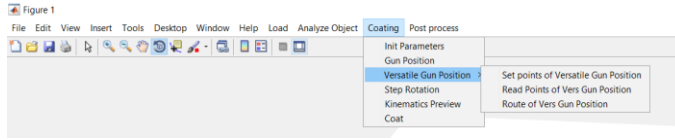
This selection allows the user to perform a more complicated gun positioning, as following:

- The user may select any number of vertices on the surface of the object
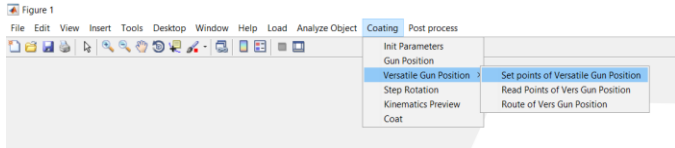
As shown in Fig.(3.15) every point that the user selected is depicted as a red star in the object and a text box appears in the lower right corner of the figure. By pressing the "OK" button the points are saved in a matrix.
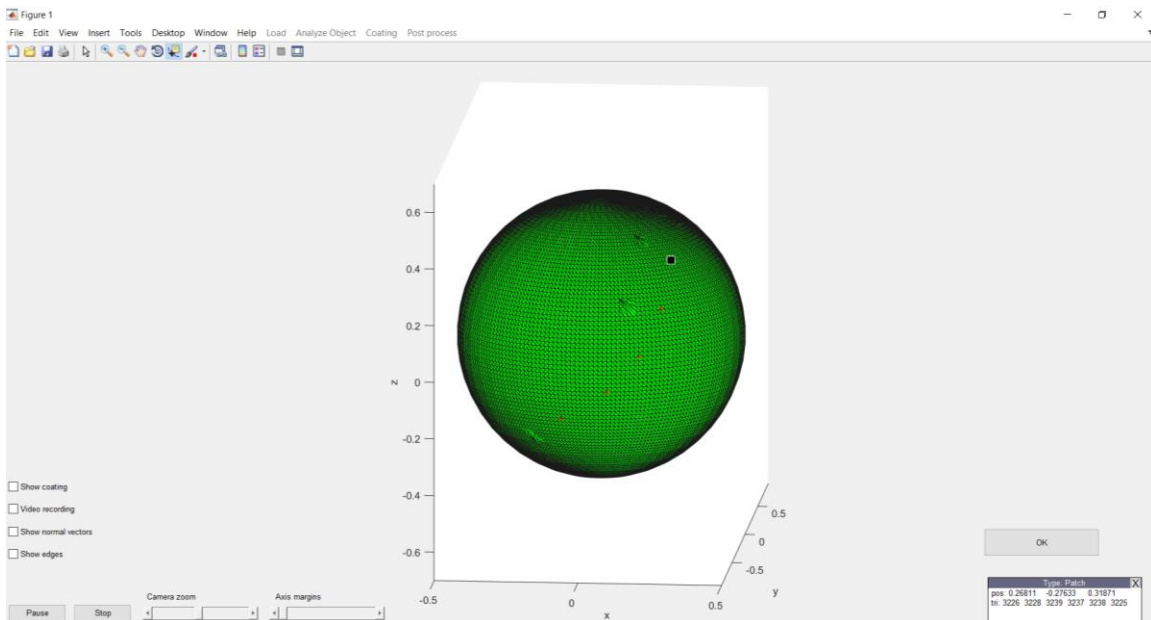
Figure 3.15 Selection of free hand points

- For each selected point, a gun pose is generated by placing the gun at a default distance from the point along the surface local normal vector and orienting the gun to point at the selected vertex.
- A gun trajectory is calculated by moving the gun at preselected default speed through each generated position. The pose (position and orientation) and speed is linearly interpolated between the generated positions (see Fig.3.15).
- The user may set the distance and speed from each selected object vertex at any value (see Fig.3.16) using the selection "Read Points of Vers Gun Position" from the menu.

33
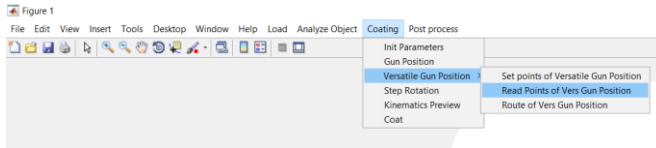
Then, a box appears that allows the user to change the default values of *SoD* and speed for each of the selected points. This box contains a drop down menu with the number (index) of the point. Every time a number is selected, the coordinates of the specific point appear. There is also a scroll bar, that changes the value of *SoD*, as well as a text box in which the user inserts the speed value that the gun should have while passing above and coating the selected point. By pressing "OK" those parameters are saved and the box closes.
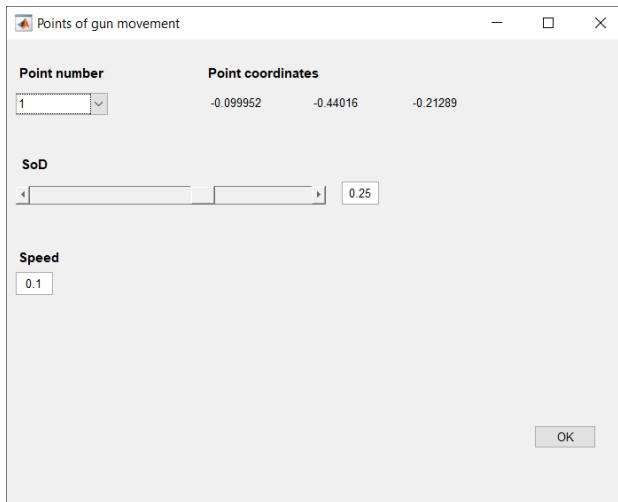
Figure 3.16 Modal window for selecting SoD and speed for every selected point in free hand mode

- The next step is a visual representation of the route of the gun as shown in Fig.(3.17). The red vectors represent the direction of the beam while coating the selected points. The blue lines show the gun's position in every iteration. The pun posistion and orientation at the intermediate points of the trtajectory are calculated using linear interpolation.

34
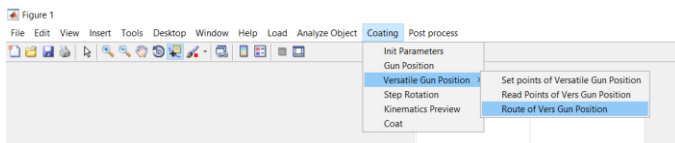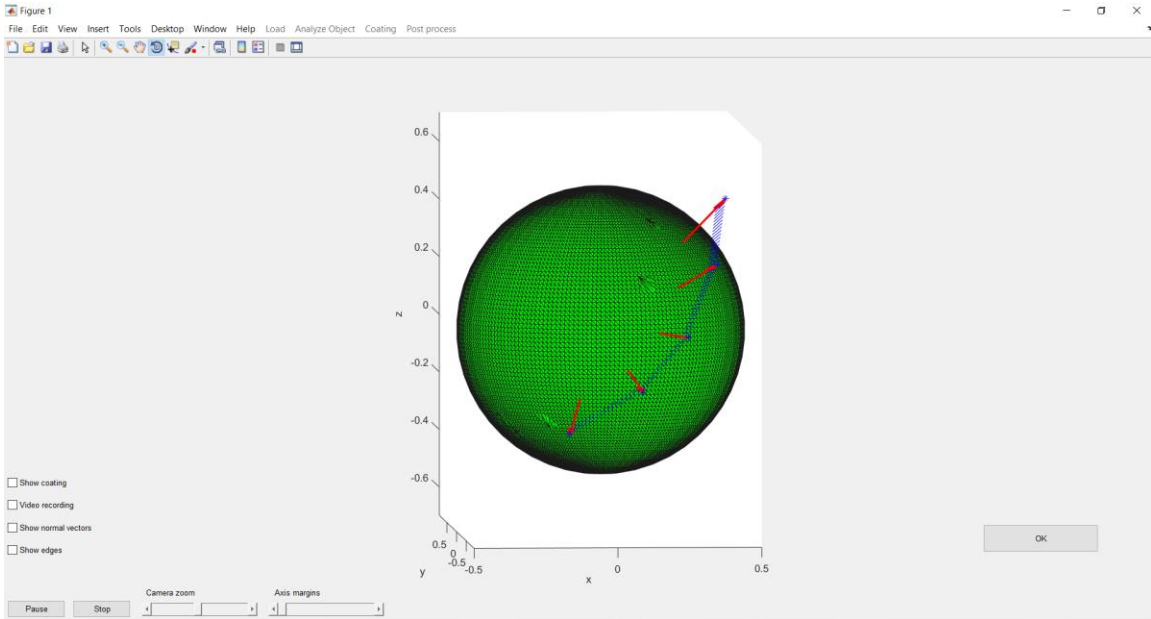
Figure 3.17 A visual representation of the route of the gun, passing from all the selected points in free hand mode

With the selected points above, as a sample, a coating process was performed as shown in Fig.(3.18). As it can be seen, the gun smoothly changes its position, thus even complicated surfaces can be coated using this method.
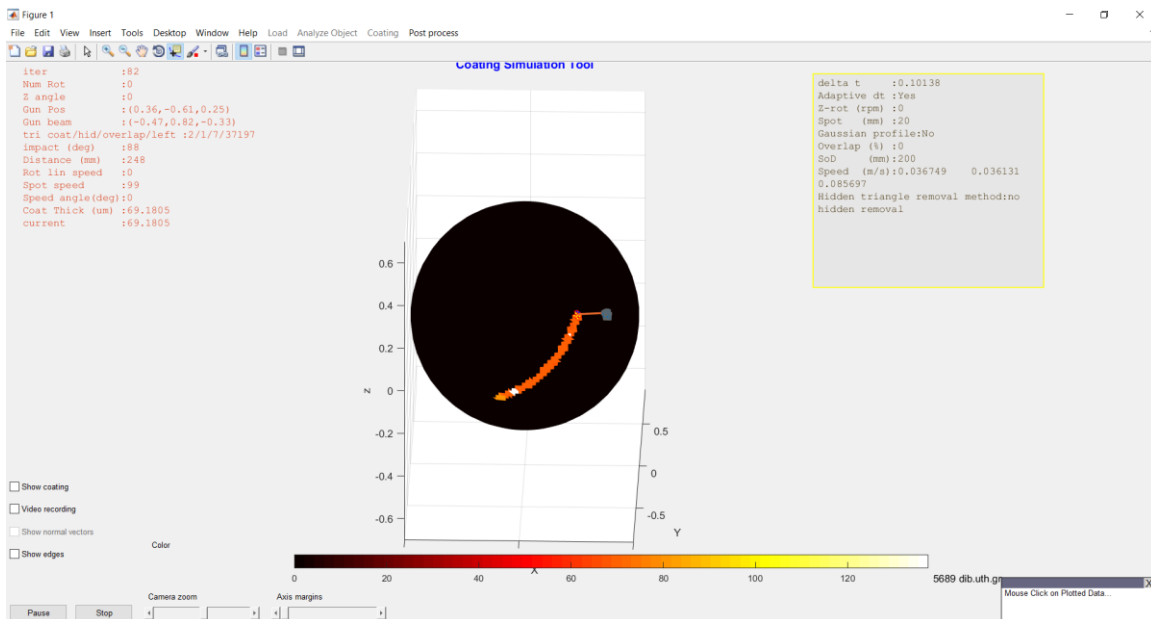
Figure 3.18 The process of coating in free hand mode
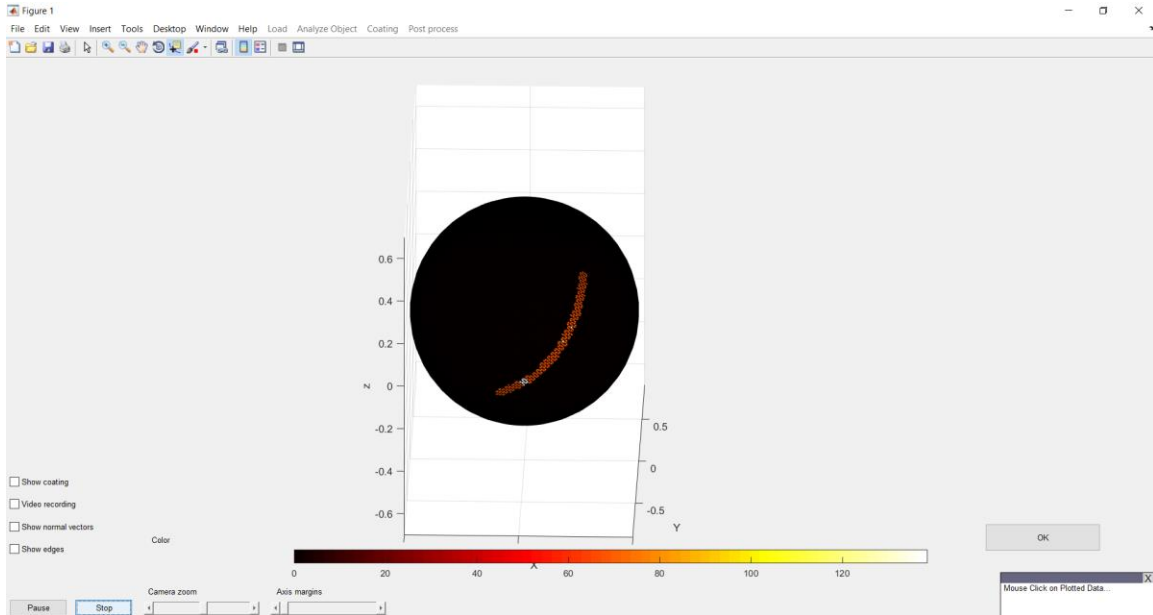
Figure 3.19 Inspection of free hand coating in a sphere

"Step rotation"
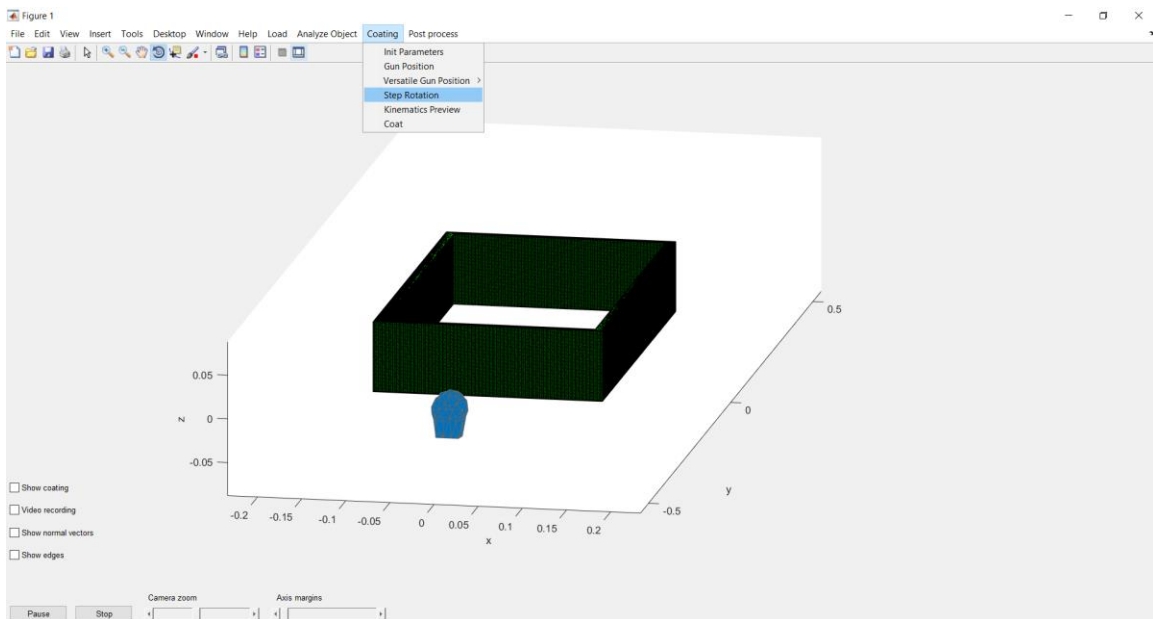
Figure 3.20 The original position of the billet in 0^0

Step rotation can be performed at the beginning or in the middle of the coating process. This feature allows the user to interrupt the coating process, change the current rotation of the object and continue the process, or start a new one. The required angle can be set using a bar that appears under the object, once this selection is activated, or by directly inputing the value of the

36

angle in degrees in the relevant textbox. A typical example of this feature is shown in Fig.(3.21), setting the object's step rotation at an angle of 30^0.
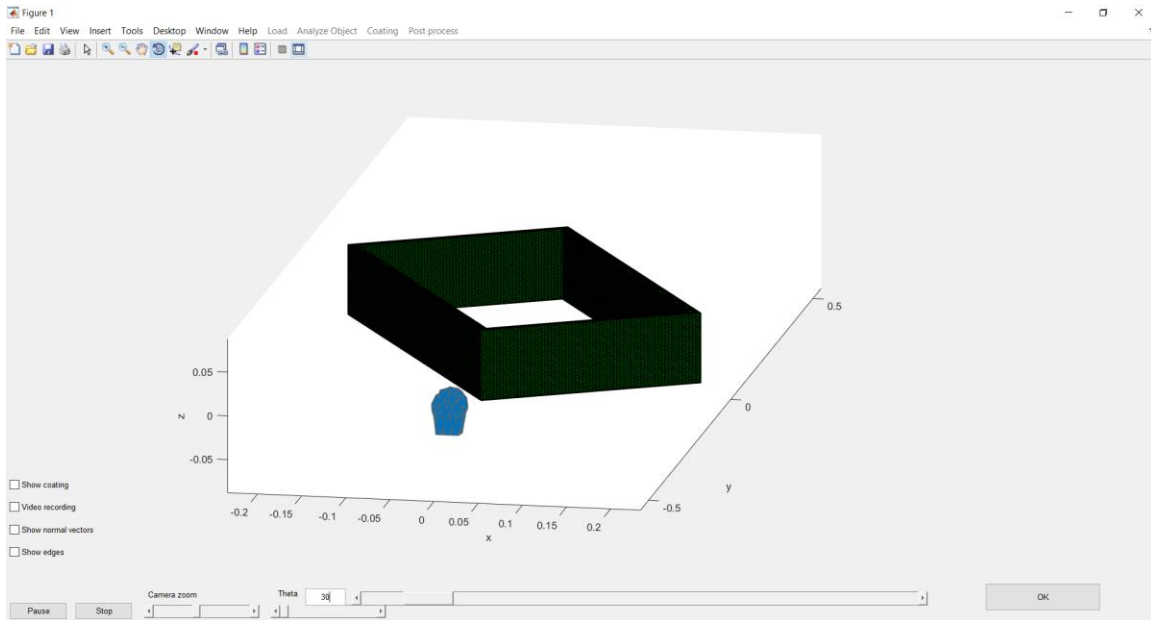
Figure 3.21 The billet after a 30^0 step rotation

"Kinematic preview"

This feature allows a quick preview of the movement of the nozzle and the object, without performing coating, so that the user may verify the planned process before the actual simulation.
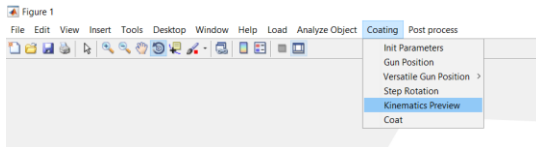
In Fig.(3.22), the red frame indicates the boundaries of the movement of the nozzle, which were determined before in "*Z Selection*" and "*Horiz Selection*". The time step is also used in the preview feature, however, there is no requirement for accurate δt calculation, since the purpose of the feature is to provide a fast and approximate verification of the kinematics. Thus, a bar is provided below the object that allows the user to change the time step and set it to large values, even during the preview. The route of the gun is a red line inside the box. The blue line shows the direction of the beam.

37
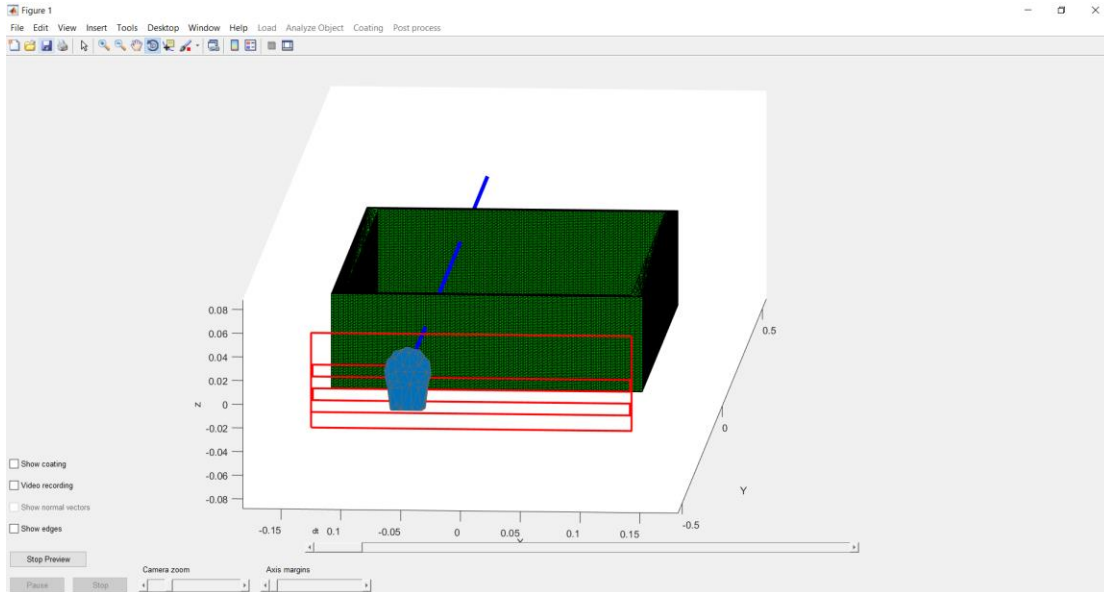
Figure 3.22 Kinematic preview of the gun movement

"Coat"

In this selection, the coating simulation is performed and visualized, providing information for all parameters in each iteration. The current thickness is displayed for each elementary triangle of the object, using color encoding.
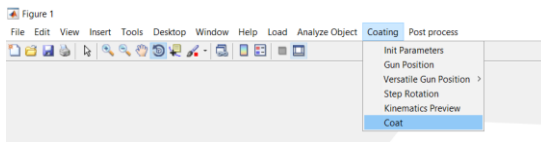
As it is shown in Fig.(3.23), there are some other options provided, as checkbox in the lower left corner. After the coating process, the user can see the surface coated, when the option is selected. Having selected the "Video recording" option during the coating, the process is saved in frames, in a folder selected by the user. Other features provided to help the user are the visual representation of the normal vectors of the object's barycenters, which is deactivated during the coating, and the option to show or hide the mesh grid of the substrate. The software supports "PAUSE" and "STOP" of the coating operation. During coating certain menu selections are disabled.

38
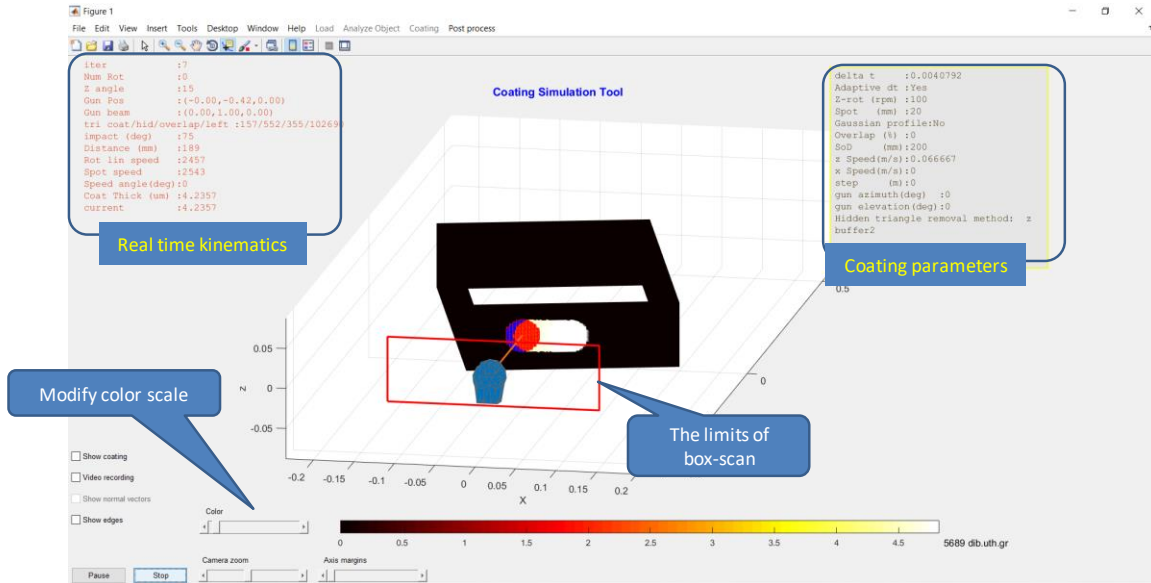
Figure 3.23 The appearance of the application window during the process of coating a billet. Some of the main features have been indicated.

3.4 Post process

This menu collects a set of options necessary for inspecting the resulting coating of the substrate.

"Inspect"

After the end of the coating process, the thickness, the impact angle, the distance from the gun and the linear speed for each triangle can be retrieved.
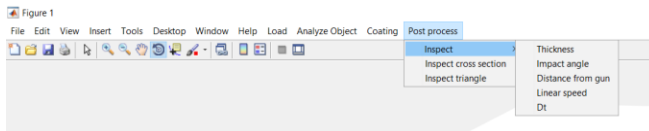
The user can see these kinematic parameters for each triangle are displayed on the substrate using color encoding. Figure 3.24 shows the coating thickness. The color bar below the object shows the range of values of the colormap. The user can change the maximum value mapped in white color, using the scroll bar in the left. The user may display in this way any one of the parameters of the coating process that appear in the 2nd lever submenu: Thickness, impact angle, SoD, Spot speed and δt.

Please note that for each triangle, the displayed value of the selected parameter is the average value considering all the iterations that his triangle was "seen" by the gun's beam.
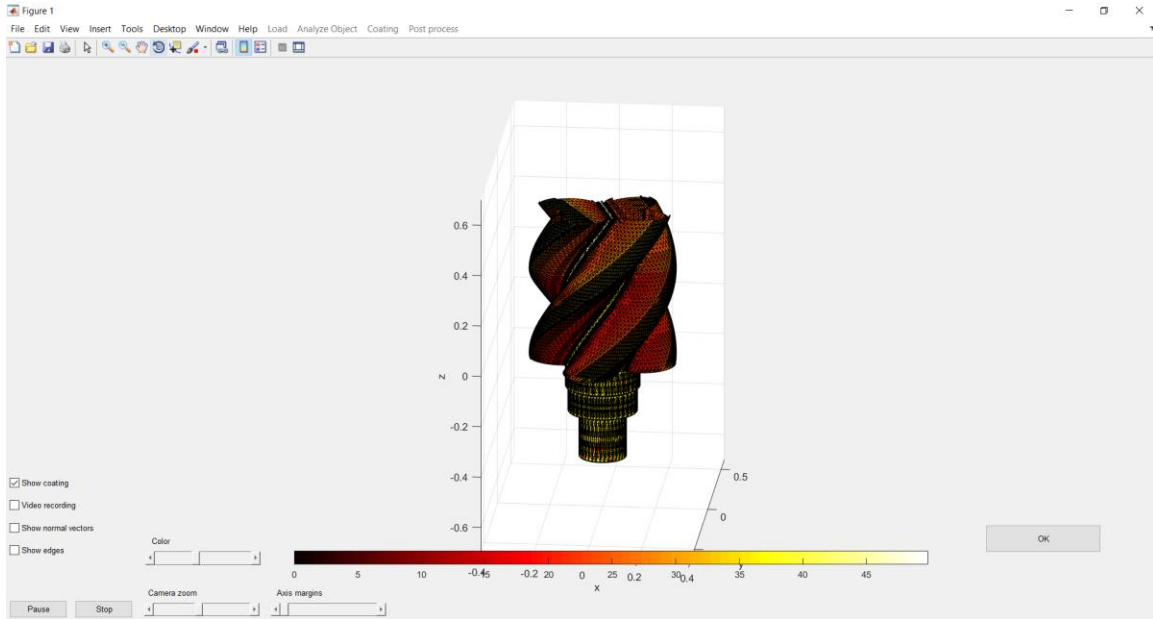
Figure 3.24 Inspection of coating thickness in color

"Inspect cross section"

This feature provides the capability to examine the coating thickness as a graph for any horizontal cross section in a different window, as shown in Fig.(3.25). The graph shows the values of thickness for the points that belong to the same horizontal plane of the object. Moving the scroll bar changes the plane of used for the cross section, in real time. This option can be combined with the "Orientation" feature to generate and inspect cross sections in any one of the three main Cartesian planes.

Pressing the "Close" button will delete the new window and the scroll bar.

40
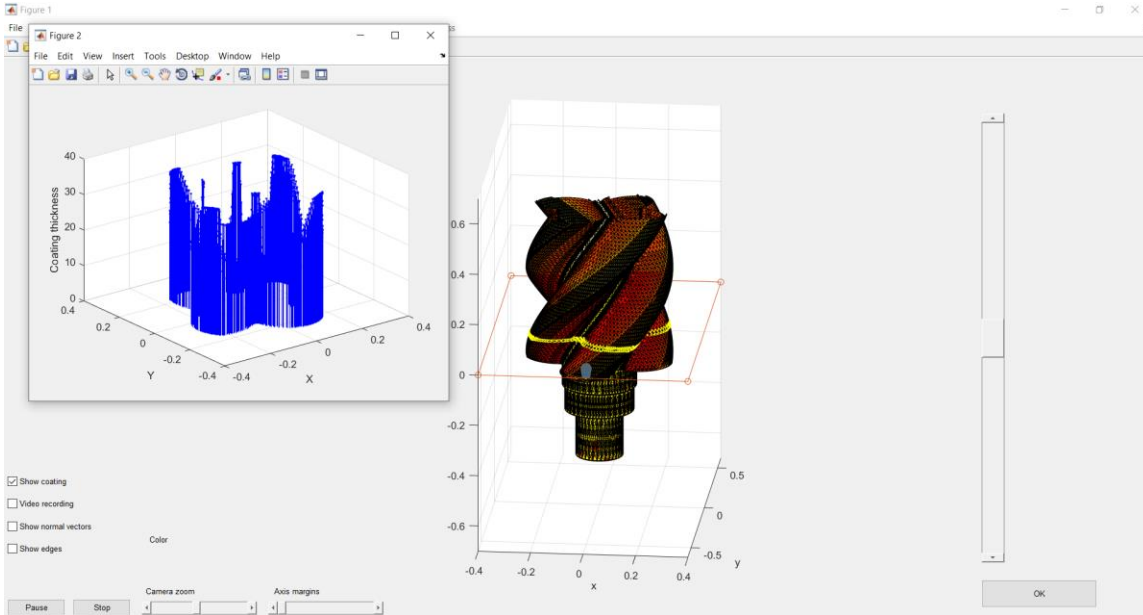
Figure 3.25 Inspection of the thickness of the rotor using the "Inspect cross section" tool

"Inspect triangle"

This feature allows the user to inspect the details of coating of any elementary triangle, selected by the mouse, at each iteration.
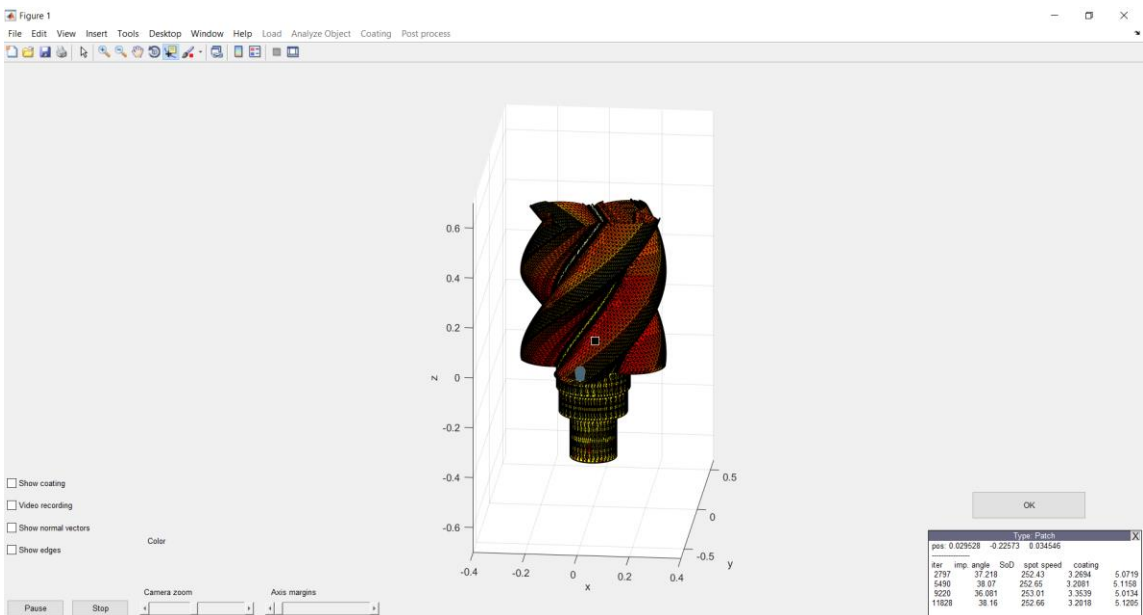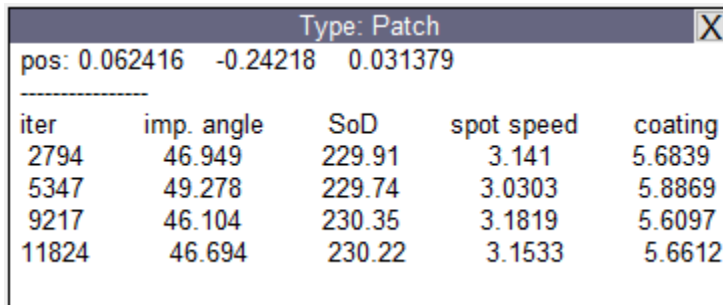
Figure 3.26 The feature "Inspect triangle"

41

After a triangle is selected, the relevant information appears in tabular form at the lower right corner of the application window. First the position (Cartesian coordinates) of the triangle's barycenter is displayed, followed by a table that contains information about the specific triangle selected by the user. Each triangle is usually coated in more than one iteration. Therefore, each line in the table provides data for each iteration. The first column shows the iteration number during which the triangle was sprayed. The rest of the columns show the impact angle, SoD, spot speed and the resulting coating thickness, for each iteration.

Pressing the "*OK*" button, closes the triangle information window and exits this inspection mode.

		Type: Patch		X
pos: 0.062416	-0.24218	0.031379		
---------------				
iter	imp. angle	SoD	spot speed	coating
2794	46.949	229.91	3.141	5.6839
5347	49.278	229.74	3.0303	5.8869
9217	46.104	230.35	3.1819	5.6097
11824	46.694	230.22	3.1533	5.6612

4. Results

4.1 Computational Complexity

If N_T is the number of triangles, the complexity for the four main steps that are repeated through the process are:

- Update object rotation $O(N_T+N_V)$
- Identification of elementary triangles inside the beam $O(N_T)$
- Hidden triangle detection $O(N_T^2)$
- Interpolation $O(N_T)$

This software has been developed using the Matlab programming environment, without utilizing any kind of parallelization (multi-thread, or GPU programming), other than Matlab's implicit parallelism. Assuming an object that consists of 10^5 elementary triangles and a beam spot size that contains approx. $10^1 - 10^2$ triangles, with all the features enabled (hidden triangle removal, Gaussian profile etc) each iteration requires about 0.1 sec when executed on a high-end laptop (i7 @3GHz, 8 GB RAM).

4.2 Rotational coating experiment of a vertical plate

The rotational experiment described in subsection 2.2 of [1] and illustrated in Fig. (2a), (2b) of [1] is simulated using the proposed TCS tool. Kinematic and operational settings were set in the simulator and the measurements presented in [1] were reproduced as following:

The geometry of the experiment in [1] was recreated in the simulation using the parametric equation of a square cross section short tube with dimensions 420x240 mm, with its center of mass placed at the start of the reference axis system. Surface triangulation was performed in the surface parameter space. The gun was placed at the origin of the reference axis system. Thus the two long sides have the identical ideal geometry of the setup being simulated

- the SoD=120mm at the center of the plate with beam impact angle of 90^0 and
- at the edge of the plate: SoD=240mm with beam impact angle=30^0.

Five (5) sites on the substrate were selected, according to beam's impact angle. The spot speed and the stand of distance (SoD) were calculated, using the simulator, and the calculated values may deviate from the ideal ones due to the non-zero beam radius r_o as well as due to the triangulated nature of the substrate surface. The 5 testing sites are visualized in our simulation in Fig.(4.1), labeled as S1 to S5, using the nomenclature of [1]. The frequency of Z-axis rotation was set to 40rpm. The simulator tessellates the plate (or any surface) into elementary triangles, so a small number of triangles exist at each one of the testing sites of the substrate.
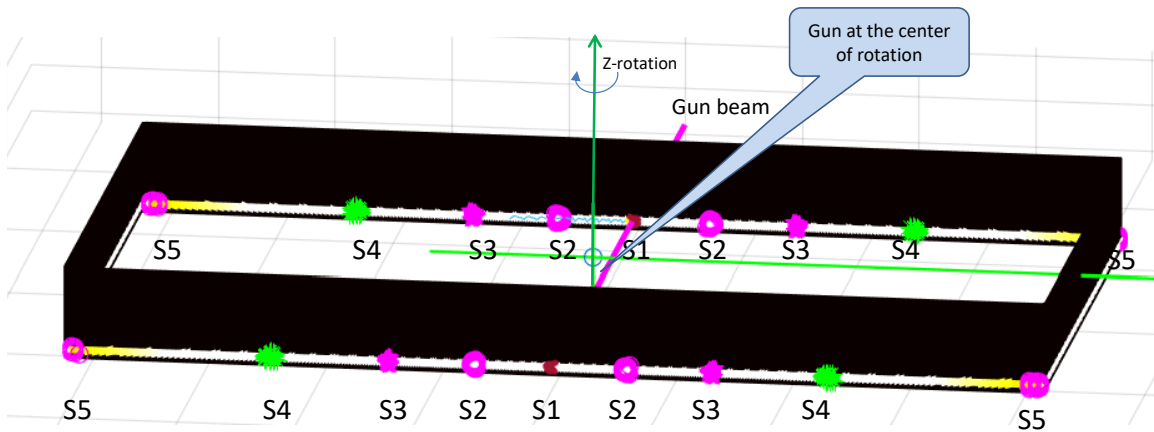
43

Figure 4.1 The 5 testing sites, defined in [1], visualized on our coating simulation setup. Please note that the two long sides of the substrate have identical setup with the rotational experiment in [1].

Subsequently, the coating thickness was calculated and averaged over the number of beam passes over each site. The resulting simulation of the coating is shown in Fig.(4.2) using color encoding, as indicated by the relative color-bar. Since the gun remains still (at the center of rotation) during the coating process, the number of rotations only affects the absolute value of the coat thickness, not the relative thickness of each site with respect to site S1 (the one with impact angle=90^0). The relative thickness of the other 4 sites with respect to S1 is compared with the experimental measurements.
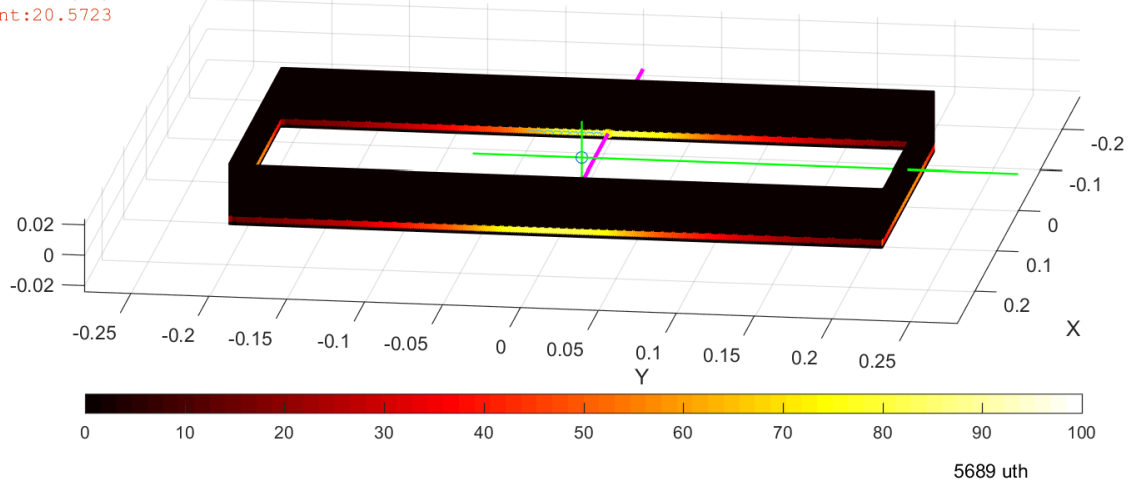
Figure 4.2. The final frame of the coating process. The two large sides of the parallelepiped have identical geometric setup with the rotational experiment in [1]. The coating thickness is color encoded (in µm).

Table I. Comparison of the calculated kinematic parameters and the relative thickness by the proposed simulator, with the experimental results, for the 5 sites (with respect to S1) as reported in [1].

Site	Impact angle [0]	SoD (mm)		Linear Speed mm/s		Coating thickness		Coating thickness relative to S1	
		Simulation	[1]	Simulation	[1]	Simulation	[1]	Simulation	[1]
S1	90	120.0	120	502.7	502	371.64	373	1.0000	1.0000
S2	75	124.3	124	539.4	538	336.11	340	0.9044	0.9115
S3	60	138.5	138	670.0	670	220.80	262	0.5941	0.7024
S4	45	169.3	170	1000.9	1005	139.96	160	0.3766	0.4290
S5	30	237.4	240	1973.7	2010	61.57	71	0.1657	0.1903

It can be observed that the SoD and Spot speed calculations of the simulator are in very good agreement with the values provided in [1]. The Coating thickness relative to S1, calculated by the simulator is also accurate compared to the experimental measurements. Fig.(4.3) illustrates the accuracy of relative coating thickness calculation for the sites of the substrate selected in [1], with respect to S1. The five data points of Fig.(4.3) correspond to the 5 testing sites S1 – S5, as described above. As it can be observed in the last two columns of Table I and the graph in Fig.(4.3), the simulated coating thickness is in very good agreement with the experimental results for all testing sites.
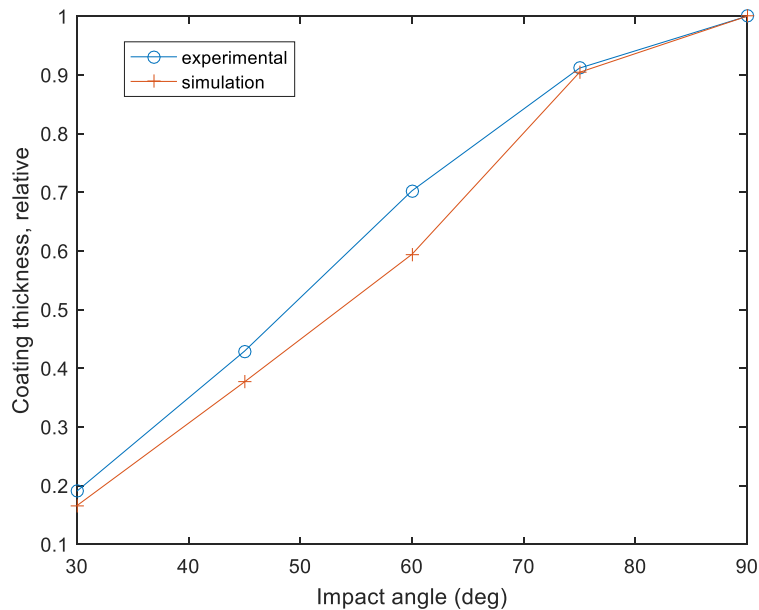
Figure 4.3 The comparison between calculated decrement of coating thickness relative to S1 (impact angle of 900), simulated by the developed simulator and measured experimentally as in [1].

45

4.3 Results in more general scenarios

Using the "Inspect cross section" tool for the simulated coating thickness, the impact angle of the beam, the distance of the object from gun, the linear speed and the adaptive dt for several substrates are examined.

The first coated object is a sphere and two different coating scenarios are shown below.

Scenario 1

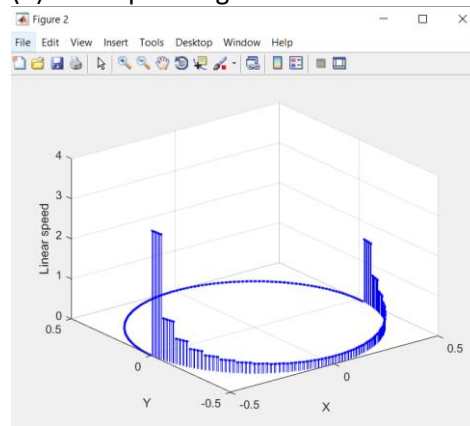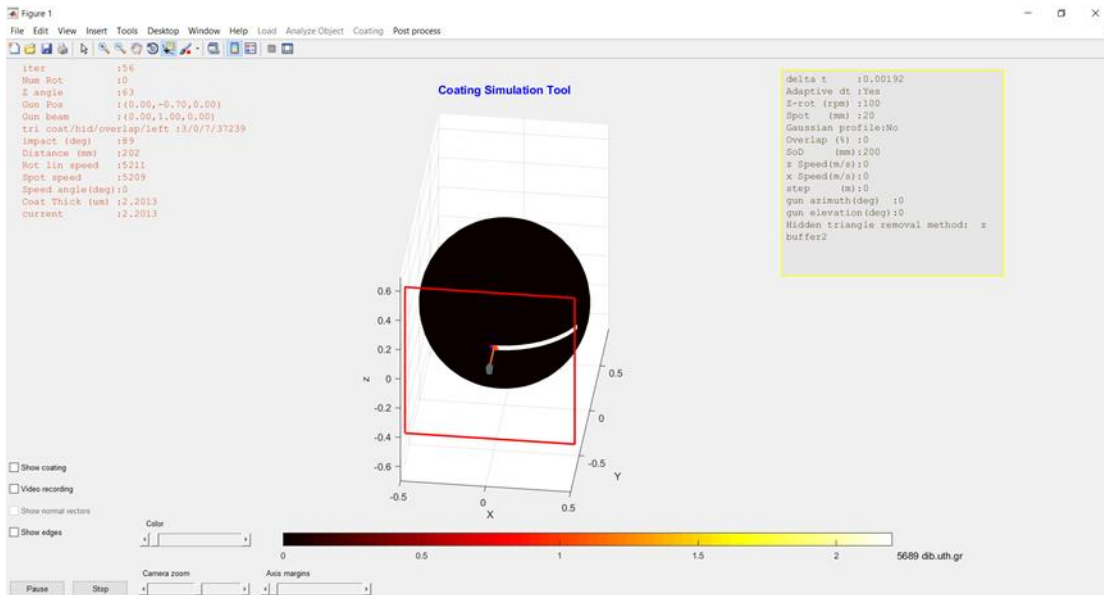| Substrate	Sphere
Object rotation (rpm)	0
Gun vector speed (m/s)	0.2
Spot radius (mm)	20
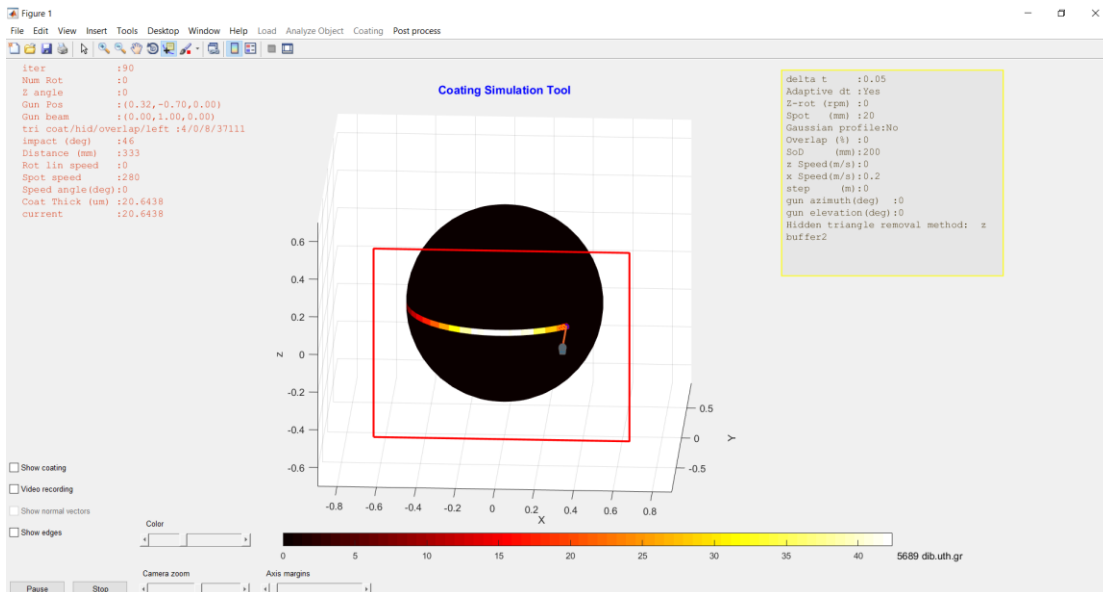
*Figure 4.4 The calculated coating thickness, overlaid in color on the actual positions of the sphere*
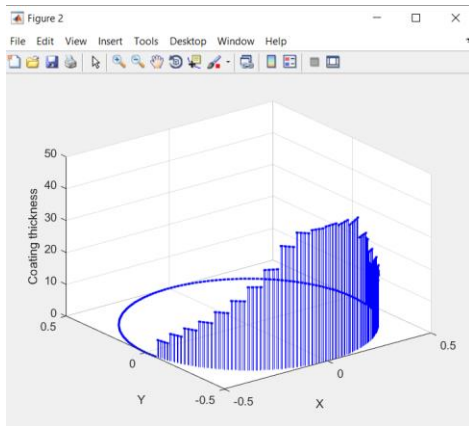
(a) the simulated coating thickness
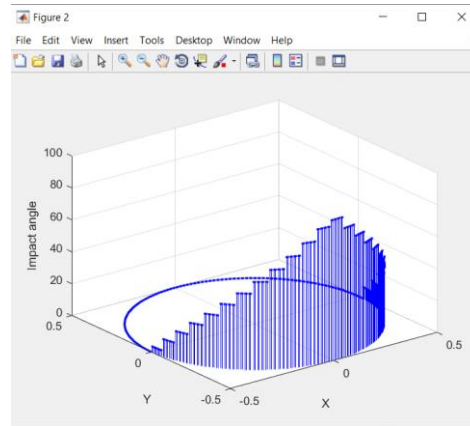
(b) the impact angle of the beam
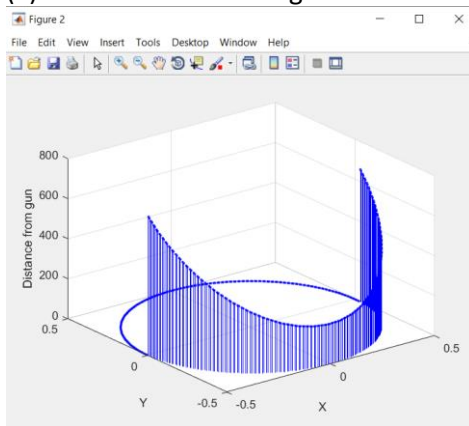
(c) the distance of the object from gun

(d) the spot speed
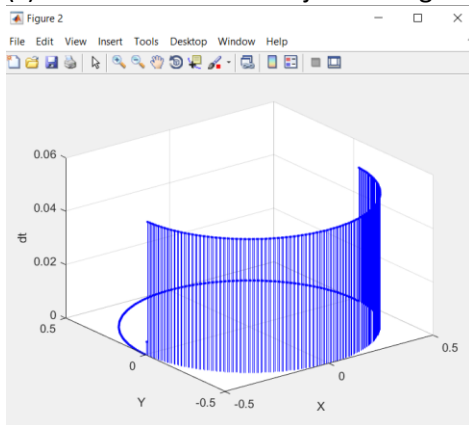
(e) the adaptive δt

Figure 4.5 Inspection of the coating parameters in a still sphere with gun movement 0.2m/s and a spot radius 20mm

In the first scenario, the sphere is still while the gun is moving in the X axis with a speed of 0.2 m/s from one end of the object to the other, only once. As shown in Fig.(4.5a), the coating thickness increases with a steady rate until the gun approaches the center of the sphere in X axis, where it changes slightly for a few iterations until the gun starts to move away from the center again, with thickness decreasing in a symmetric manner.

The same happens to the impact angle of the beam, which approaches 90^0 near the center of the X axis, where the beam reaches the surface almost vertically. As the gun is moving straight the

47

vertical distance from the sphere changes as shown in the diagram(c), with the minimum value equal to the SoD (200mm), set by the user.

The spot speed is equal to the gun speed (0.2 m/s) only at the point of vertical impact, whereas its value increases exponentially towards the limits of the movement, where the impact angle approaches 0.

As expected from Eq.(2.13), adaptive δt was constant during the whole process.

Scenario 2

| Substrate	Sphere
Object rotation (rpm)	100
Gun vector speed (m/s)	0
Spot radius (mm)	20

Figure 4.6 The calculated coating thickness, overlaid in color on the actual positions of the sphere
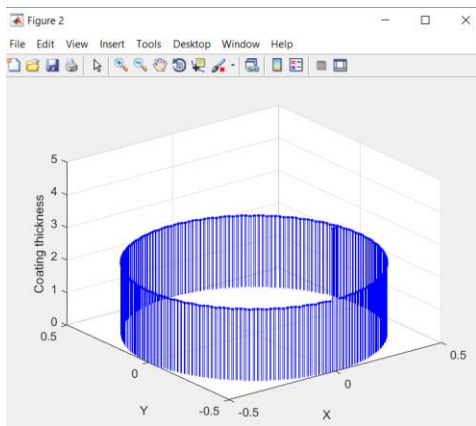
(a) the simulated coating thickness
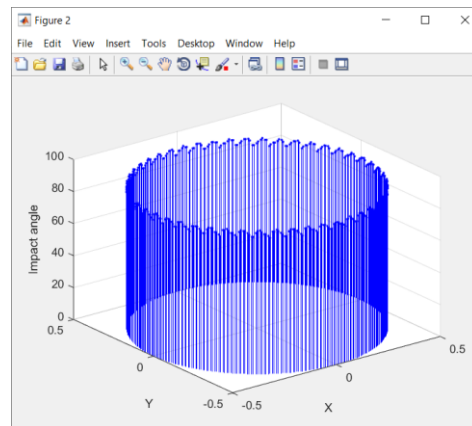
(b) the impact angle of the beam
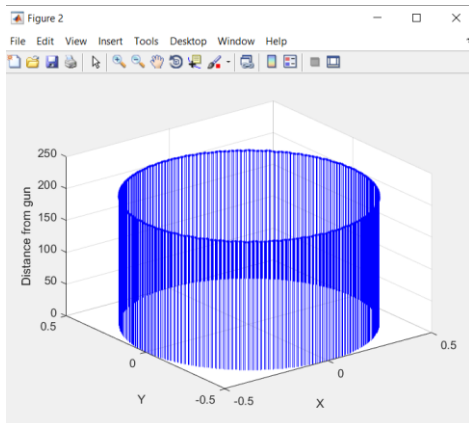
(c) the distance of the object from gun
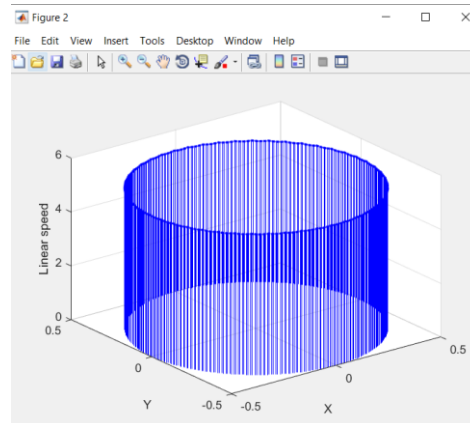
(d) the spot speed
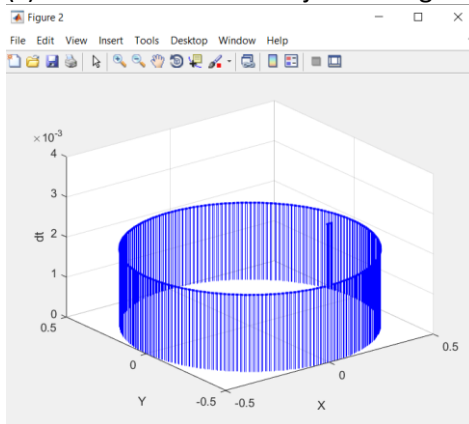
(e) the adaptive δt

Figure 4.7 Inspection of the coating parameters in a sphere rotating at 100 rpm with a still gun and a spot radius 20mm

In the second scenario, the sphere is rotating at 100 rpm, while the gun is still. As shown in Fig.(4.7), all the parameters are constant since the object is symmetrical and the gun sees the same number of triangles in each iteration, from a steady SoD (Fig.(4.7c)), defined by the user. No change of the impact angle is recorded, as expected (Fig.(4.7b)). The elementary time δt also remains constant at 2msec, as also expected.

50

Scenario 3

Substrate	Billet
Object rotation (rpm)	40
Gun vector speed (m/s)	0
Spot radius (mm)	5

In this scenario, a rotating rectangular box is being coated externally by a still torch, as shown in Fig. (4.8).
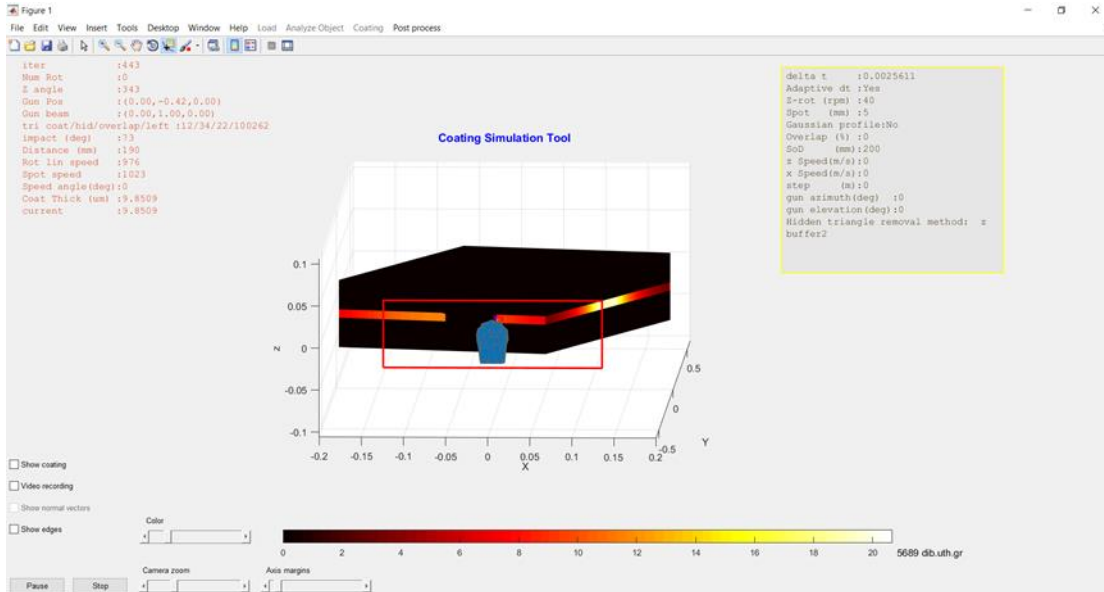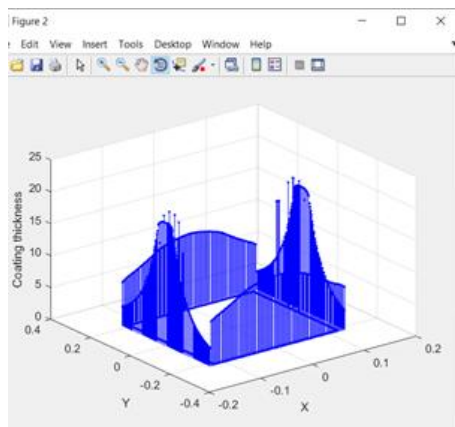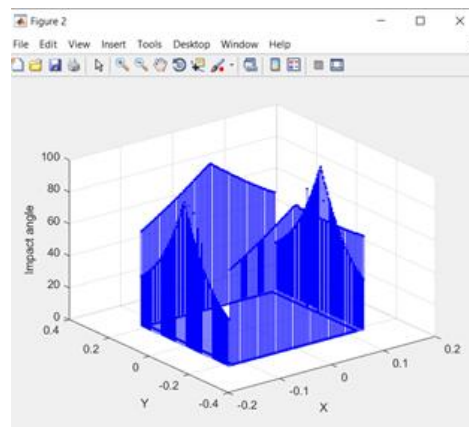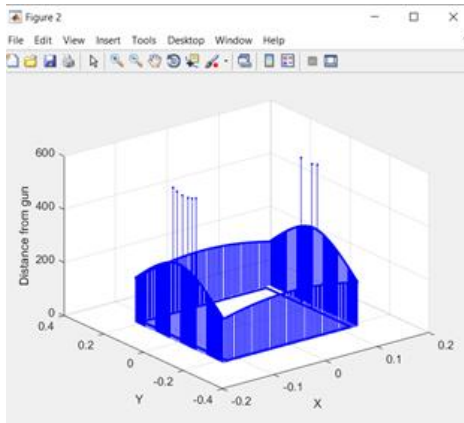

Figure 4.8 The calculated coating thickness, overlaid in color on the actual positions of the billet
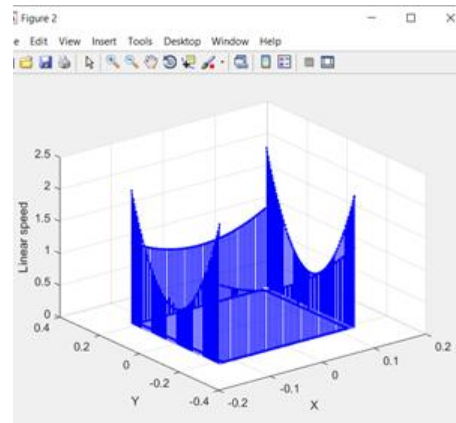

(a) the simulated coating thickness

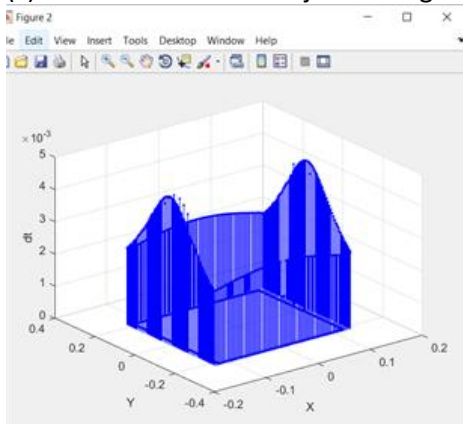
(b) the impact angle of the beam

(c) the distance of the object from gun

(d) the spot speed

(e) the adaptive δt

Figure 4.9 Inspection of the coating parameters in a billet rotating at 40 rpm with a still gun and a spot radius 5mm

The billet rotates at 40 rpm while the gun is still. Because of the billet's geometry, the results are the same for the pairs of parallel sides of the object. In Fig.(4.9a), the coating thickness in the two parallel sides with the shorter length increases until the gun approaches the center of the sphere in X axis, where it changes slightly for a few iterations until the gun starts to move away from the center again, where it decreases again. The coating thickness changes the same way for the two remaining sides, but with a different rate and with a smaller maximum value.

The impact angle of the beam in the surface, increases almost linearly for all the sides of the billet, with a higher rate in the shorter sides. At the middle of the each side, the impact angle is 90^0 as expected. The distance of the gun from the billet changes as shown in the diagram(c). The spot speed (with respect to the surface being coated) is lower when the gun sprays the center of the sides and significantly higher at the edges of the sides. During the spraying of the shorter sides the time step is higher than when spraying at the other sides of the object, due to the higher linear rotational speed of the surface.

52

Scenario 4

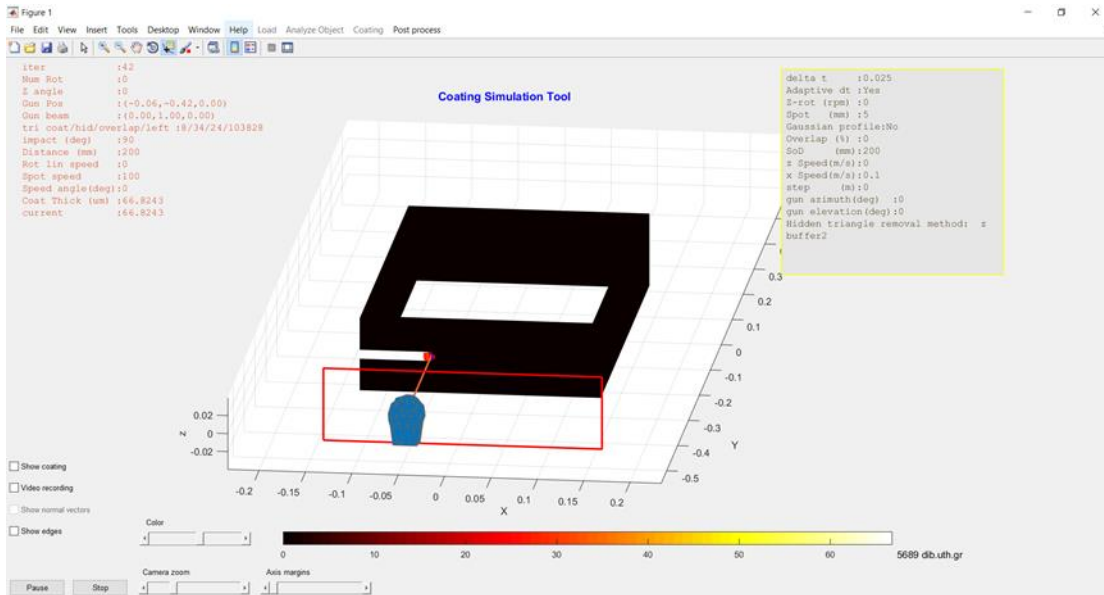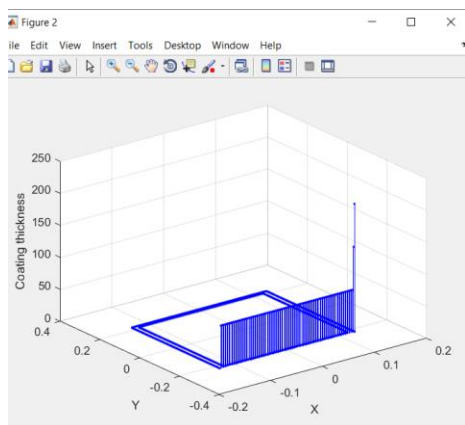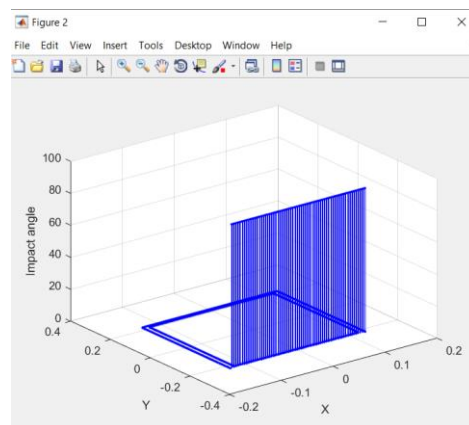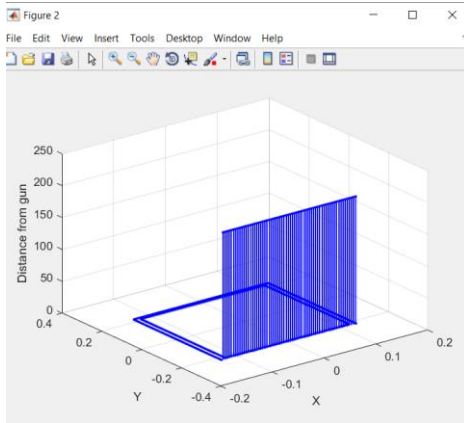| Substrate	Billet
Object rotation (rpm)	0
Gun vector speed (m/s)	0.1
Spot radius (mm)	5

Figure 4.10 The calculated coating thickness, overlaid in color on the actual positions of the billet
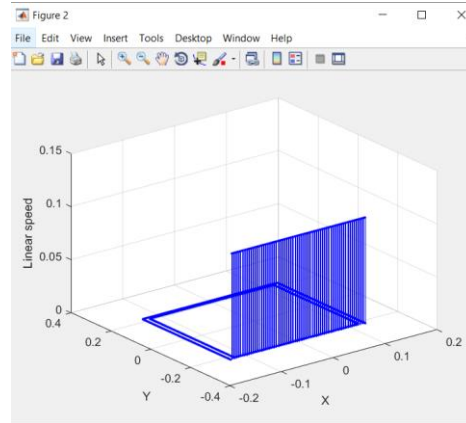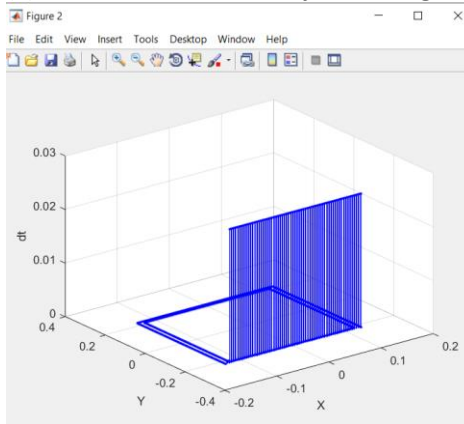

(a) the simulated coating thickness   (b) the impact angle of the beam

(c) the distance of the object from gun

(d) the spot speed

(e) the adaptive δt

Figure 4.11 Inspection of the coating parameters in a still billet with gun movement 0.1m/s and a spot radius 5mm

In the fourth scenario, the billet is still while the gun is moving in the X axis with a speed of 0.1 m/s from one end of the object to the other, only once. As shown in the Fig.(4.11) , all the parameters are have constant values with an impact angle at 90^0 , the SoD at 200 mm and spot speed equal to the gun speed at 0.1 m/s, as expected given the initial parameters set by the user.

54

Scenario 5

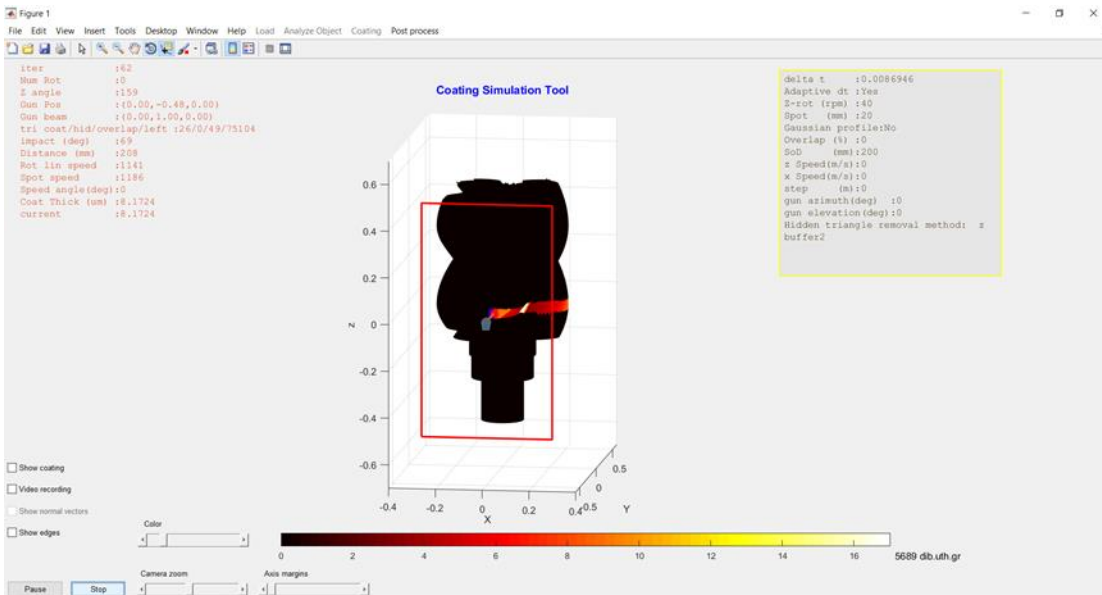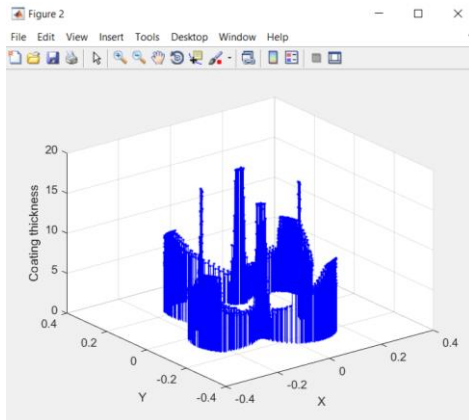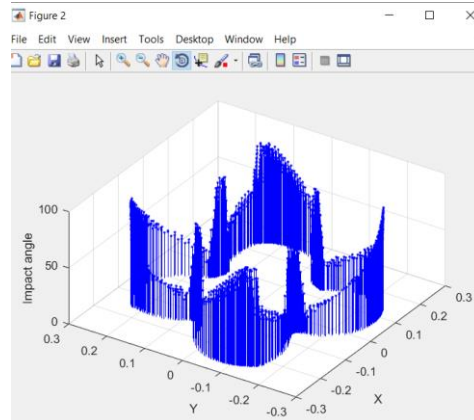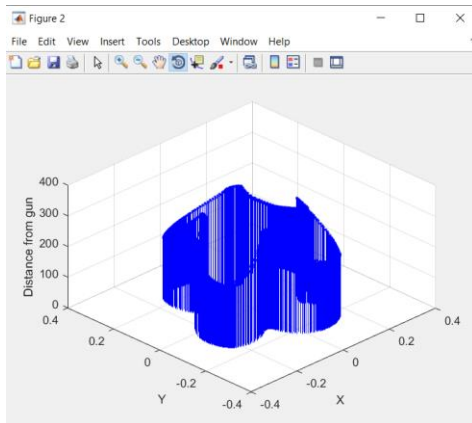| Substrate	Rotor
Object rotation (rpm)	40
Gun vector speed (m/s)	0
Spot radius (mm)	20

Figure 4.12 The calculated coating thickness, overlaid in color on the actual positions of the rotor
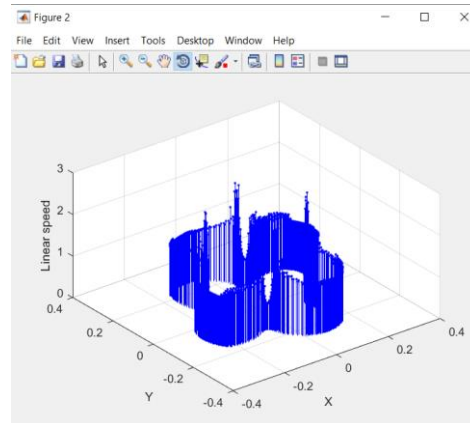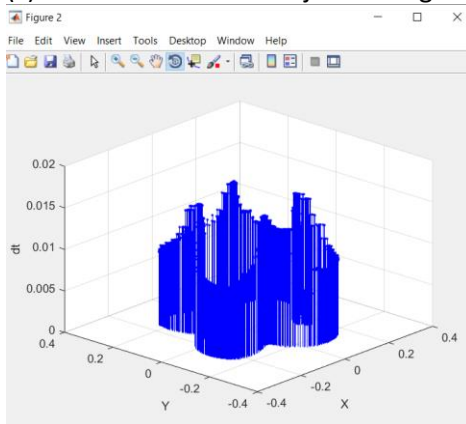

(a) the simulated coating thickness   (b) the impact angle of the beam

55

(c) the distance of the object from gun

(d) the spot speed

(e) the adaptive δt

Figure 4.13 Inspection of the coating parameters in a rotor rotating at 40 rpm with a still gun and a spot radius 20mm

Finally, in the fifth scenario, the rotor is rotating at 40 rpm and the gun is still. The changes on the parameters are due to the geometry of the substrate. The higher values of coating thickness (Fig.(4.13a)) are observed inside the folds of the rotor as the impact angle there is almost 90^0, as shown in Fig.(4.13b). The distance of the gun changes the same way, as well as, the linear speed and the adaptive time step.

4.4   The effect of the Gaussian profile

The Gaussian radial profile of the intensity of the beam has been implemented, in order to allow for realistic simulation, where the main requirement is the uniform coating thickness. The effect of the implemented Gaussian profile is demonstrated in the following comparative experiment.

A sphere and a rotor were sprayed using the same settings: the rotation frequency of the substrates is set to 40 rpm, the spot diameter is 4 mm and the gun movement is alongside the Z axis from the bottom up. The value of gun's Z speed was calculated for each object in order to achieve overlapping 40% of the spot diameter. In the left image of both figures the Gaussian beam profile was activated (as described in paragraph 2.5), whilst in the second one the triangles inside the beam were coated with equal intensity (flat radial beam profile). It is obvious that there is a significant difference between the two methods, with the first one giving more realistic and

56

accurate results. In real coating processes, the beam sprays in a way similar to the Gaussian profile, making overlap necessary for achieving uniformity in the resulted coating.

(a)   (b)

Figure 4.14 A sphere coated (a) with Gaussian profile and (b) without while rotating at 40 rpm with gun speed in Z axis calculated for overlap 40% of the spot diameter, which is 4mm.

(a)   (b)

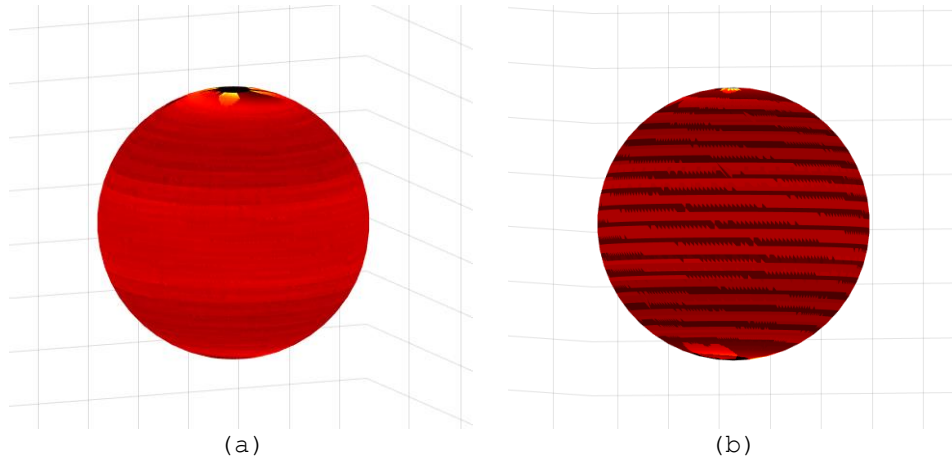*Figure 4.15 A rotor coated (a) with Gaussian profile and (b) without while rotating at 40 rpm with gun speed in Z axis calculated for overlap 40% of the spot diameter, which is 4mm.*
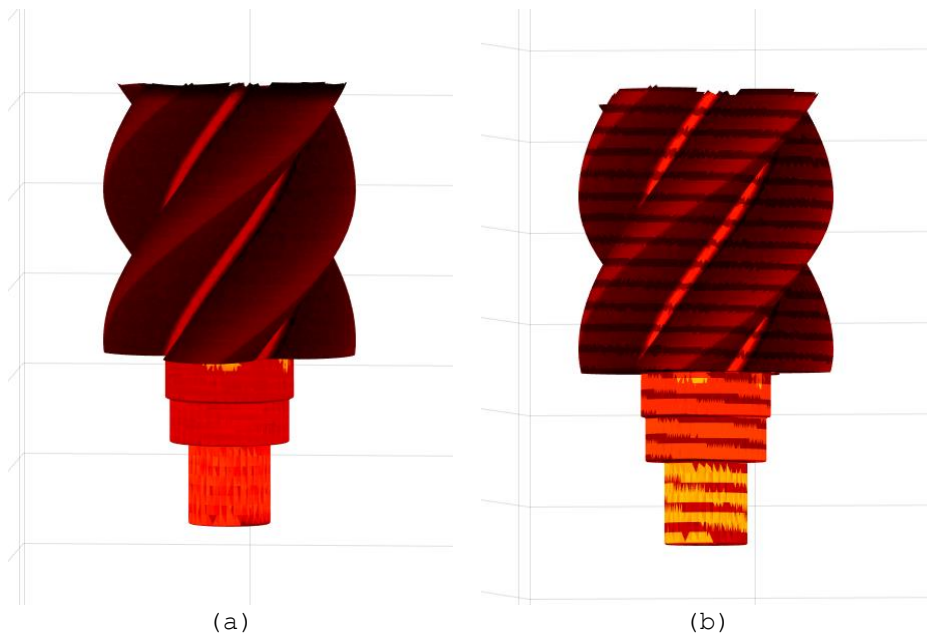
57

4.5 Coating an object with high complexity

In this section is presented a substrate of high complexity, after being coated using the simulator (Fig.(4.16)).
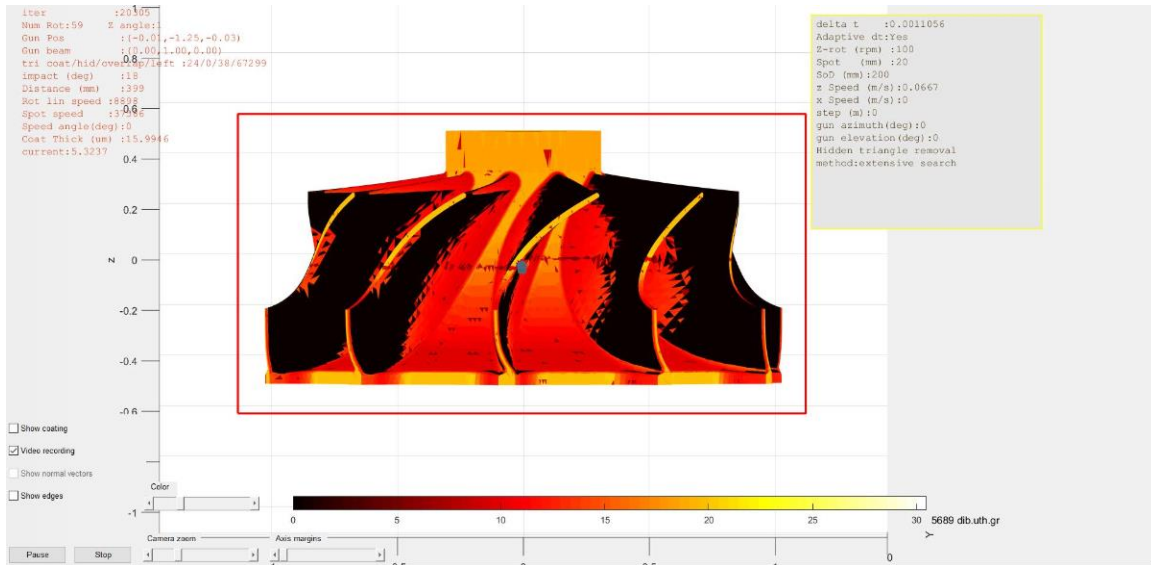

Figure 4.16 Coating thickness on an object of high complexity

5. Conclusions

A simulator for HVOF thermal coating processes was presented in this thesis, for an offline prediction of coating thickness. It is a very useful tool, easy to handle for processing surfaces of high complexity, as it provides two methods of gun movement. It integrates a number of important features in a user-friendly way, allowing for 3D object manipulation, 6 DOF gun motion, Gaussian, or flat radial profile of beam intensity, input and output of results, coating settings etc. According to the quantitative comparison of simulation results with the experimental ones, it can be seen that the simulator offers great accuracy in predicting the coated thickness. Qualitative results show that the simulator can handle very complicated objects, actually used in mechanical engineering.

One suggestion of future work is an addition to the simulator, which will allow the prediction for more than one thermal spray methods, for instance flame, or plasma coating using different powders.

Another useful extension could be the selection of the characteristics of the coated surface, except for coating thickness, porosity, micro-hardness, wear factor etc. This can be achieved by using more experimental measurements from these quantities.

From a computational point of view, a number of optimizations source code may be perform in order to accelerate the performance of the software: rewrite certain functions in a low-level, faster programming language, utilize multi-thread programming, or GPU programming in a single computer platform, or in a cluster of computers.

Furthermore, an extension after the above point would be integrate the simulator with a number of sensors (mainly position ones) to allow the use of the simulator for online tracking of the production process using the current gun position and direction, providing a tool for controlling and checking the process in real time.

Finally, the simulator could serve as the basis for building an artificial intelligence system, or a machine learning system that solves the inverse coating problem: given an object to be coated, it may propose an efficient kinematic model that achieves the desired coating characteristics.

6. References

[1]   Katranidis, Vasileios, Sai Gu, Bryan Allcock, and Spyros Kamnis. "Experimental study of high velocity oxy-fuel sprayed WC-17Co coatings applied on complex geometries. Part A: Influence of kinematic spray parameters on thickness, porosity, residual stresses and microhardness." *Surface and Coatings Technology* 311 (2017): 206-215.

[2] Katranidis, Vasileios, Sai Gu, Tomas Ramirez Reina, Esat Alpay, Bryan Allcock, and Spyros Kamnis. "Experimental study of high velocity oxy-fuel sprayed WC-17Co coatings applied on complex geometries. Part B: Influence of kinematic spray parameters on microstructure, phase composition and decarburization of the coatings." *Surface and Coatings Technology* 328 (2017): 499-512.

[3] Katranidis, Vasileios, Spyros Kamnis, and Sai Gu. "Prediction of Coating Properties of Thermally Sprayed WC–Co on Complex Geometries." *Journal of Thermal Spray Technology* 27, no. 6 (2018): 1025-1037.

[4] Chen, Chaoyue, Hanlin Liao, Ghislain Montavon, and Sihao Deng. "Nozzle mounting method optimization based on robot kinematic analysis." *Journal of Thermal Spray Technology* 25, no. 6 (2016): 1138-1148.

[5] Hegels, Daniel, Thomas Wiederkehr, and Heinrich Müller. "Simulation based iterative post-optimization of paths of robot guided thermal spraying." *Robotics and Computer-Integrated Manufacturing* 35 (2015): 1-15.

[6] Gadow, R., A. Candel, and M. Floristán. "Optimized robot trajectory generation for thermal spraying operations and high quality coatings on free-form surfaces." *Surface and Coatings Technology* 205, no. 4 (2010): 1074-1079.

[7] Fang, D., S. Deng, H. Liao, and C. Coddet. "The effect of robot kinematics on the coating thickness uniformity." *Journal of thermal spray technology* 19, no. 4 (2010): 796-804.

[8] Deng, SiHao, ZhenHua Cai, DanDan Fang, HanLin Liao, and Ghislain Montavon. "Application of robot offline programming in thermal spraying." *Surface and Coatings Technology* 206, no. 19-20 (2012): 3875-3882.

[9] Kout, Alexander, Thomas Wiederkehr, and Heinrich Müller. "Efficient stochastic simulation of thermal spray processes." Surface and Coatings Technology 203, no. 12 (2009): 1580-1595.

[10] Tabbara, H., and S. Gu. "Computational simulation of liquid-fuelled HVOF thermal spraying." Surface and Coatings Technology 204, no. 5 (2009): 676-684.

[11] Trifa, Florin-Iuliu, Ghislain Montavon, and Christian Coddet. "Model-based expert system for design and simulation of APS coatings." Journal of thermal spray technology 16, no. 1 (2007): 128-139.

[12] Barradas, Sophie, Vincent Guipont, Régine Molins, Michel Jeandin, M. Arrigoni, M. Boustie, C. Bolis, L. Berthe, and M. Ducos. "Laser shock flier impact simulation of particle-substrate interactions in cold spray." Journal of Thermal Spray Technology 16, no. 4 (2007): 548-556.

[13] Fauchais, Pierre L., Joachim VR Heberlein, and Maher I. Boulos. "Thermal spray fundamentals: from powder to part." (2014).

[14] http://taskmaster-inc.com/thermal-spray-coatings/

[15] https://www.fst.nl/about/thermal-spray-process-what-is-thermal-spray/

[16] Davis, Joseph R., ed. Handbook of thermal spray technology. ASM international, 2004.

[17] Fauchais, P., A. Vardelle, and B. Dussoubs. "Quo vadis thermal spraying?." Journal of Thermal Spray Technology 10, no. 1 (2001): 44-66.

[18] Berger, Lutz-Michael. "Application of hardmetals as thermal spray coatings." International Journal of Refractory Metals and Hard Materials 49 (2015): 350-364.

[19] https://www.hansfordsensors.com/what-are-the-root-causes-of-wear-in-industrial-machinery/

[20] https://en.wikipedia.org/wiki/Wear#cite_note-rabinowicz-7